

Physical regimes for feedback in galaxy formation

Pierluigi Monaco

Dipartimento di Astronomia, Università di Trieste, via Tiepolo 11, 34131 Trieste, Italy - email: monaco@ts.astro.it

Accepted ... Received ...

ABSTRACT

We present a new (semi-)analytic model for feedback in galaxy formation. The interstellar medium (hereafter ISM) is modeled as a two-phase medium in pressure equilibrium, where the cold phase is fragmented into clouds with a given mass spectrum. Cold gas infalls from an external halo. Large clouds are continually formed by coagulation and destroyed by gravitational collapse. Stars form in the collapsing clouds; the remnants of exploding type II supernovae (hereafter SNe) percolate into a single super-bubble (hereafter SB) that sweeps the ISM, heating the hot phase (if the SB is adiabatic) or cooling it (in the snowplow stage, when the interior gas of the SB has cooled). Different feedback regimes are obtained whenever SBs are stopped either in the adiabatic or in the snowplow stage, either by pressure confinement or by blow-out.

The resulting feedback regimes occur in well-defined regions of the space defined by vertical scale-length and surface density of the structure. In the adiabatic blow-out regime the efficiency of SNe in heating the ISM is rather low (~ 5 per cent, with ~ 80 per cent of the energy budget injected into the external halo), and the outcoming ISM is self-regulated to a state that, in conditions typical of our galaxy, is similar to that found in the Milky Way. Feedback is most efficient in the adiabatic confinement regime, where star-formation is hampered by the very high thermal pressure and the resulting inefficient coagulation. In some significant regions of the parameter space confinement takes place in the snowplow stage; in this case the hot phase has a lower temperature and star formation is quicker. In some critical cases, found at different densities in several regions of the parameter space, the hot phase is strongly depleted and the cold phase percolates the whole volume, giving rise to a burst of star formation.

While the hot phase is allowed to leak out of the star-forming region, and may give rise to a tenuous wind that escapes the potential well of a small galactic halo, strong galactic winds are predicted to happen only in critical cases or in the snowplow confinement regime whenever the SBs are able to percolate the volume.

This model provides a starting point for constructing a realistic grid of feedback solutions to be used in galaxy formation codes, either semi-analytic or numeric. The predictive power of this model extends to many properties of the ISM, so that most parameters can be constrained by reproducing the main properties of the Milky Way.

Key words: galaxies: formation – galaxies: ISM – ISM: bubbles – ISM: kinematics and dynamics

1 INTRODUCTION

Galaxy formation is an open problem. This is due to the complexity of the feedback processes that arise from the energetic activity of massive or dying stars, taking place through winds, ionizing photons and SN explosions (not to mention AGN). These feedback processes involve a large range of scales and masses, from the sub-pc scale of star formation to the $\gtrsim 10$ kpc scale of galactic winds, and from 1 to $10^{12} M_{\odot}$ or more.

It is useful at this stage to identify ranges of scales in which different processes are dominant. On $\gtrsim 1$ kpc spatial and $\gtrsim 10^6 M_{\odot}$ mass scales the dominant processes such as shock heating of gas, radiative cooling, disc formation, galaxy merging and tidal or ram-pressure stripping are closely related to the dark-matter halo hosting the galaxy and to its hierarchical assembly. On scales ranging from ~ 1 pc to ~ 1 kpc, or from ~ 1000 to $\sim 10^6 M_{\odot}$, cool gas reaches suitable conditions for collapse and star formation, and the energy input from massive stars (through winds, UV ph-

tons and SNe) acts in shaping and sustaining the multi-phase structure of the ISM. At smaller scales star formation takes place; it is most likely driven and self-limited by magneto-hydro-dynamical (MHD) turbulence. This division is obviously meant to be only a rough approximation of reality.

Numerical simulations of whole galaxies are still limited to space and mass resolutions not much smaller than ~ 1 kpc and $10^6 M_\odot$ respectively (see, e.g., Weinberg, Hernquist & Katz 2002; Steinmetz & Navarro 2002; Mathis et al. 2002; Lia, Portinari & Carraro 2002; Recchi et al. 2002; Pearce et al. 2001; Toft et al. 2002; Springel & Hernquist 2003; Tornatore et al. 2003; Governato et al. 2004). They can address effectively the processes dominant in the large-scale range identified above, but the feedback processes acting on intermediate and small scales are “sub-grid” physics and are treated with simple heuristic models that require the introduction of free parameters.

Current models of semi-analytic galaxy formation treat feedback at a similar, phenomenological level (see, e.g., Cole et al. 2000; Somerville, Primack & Faber 2001; Diaferio et al. 2001; Poli et al. 2001; Hatton et al. 2003); they typically connect the efficiency of feedback to the circular velocity of the dark matter halo, with the aid of free parameters. Models of galaxy formation that include a more detailed description of feedback have been presented, e.g., by Silk (1997, 2001), Ferrara & Tolstoy (2000), Efstathiou (2000), Tan (2000), Lin & Murray (2000), Hirashita, Burkert & Takeuchi (2001), Ferreras, Scannapieco & Silk (2002) or Shu, Mo & Mao (2003). In this framework (semi-)analytic work can give a very useful contribution in selecting the physical processes that are most likely to contribute to feedback.

The focus of this paper is on modeling the intermediate range of scales defined above, where the physics of the ISM is in act. The standard picture of the ISM is that of a multi-phase medium in rough pressure equilibrium; the reference model is that of McKee & Ostriker (1977), who considered a medium composed by cold, spherical clouds with temperature and density $T_c \sim 100$ K and $n_c \sim 10 \text{ cm}^{-3}$, kept confined by a hot phase with $T_h \sim 10^6$ K and $n_h \sim 10^{-3} \text{ cm}^{-3}$. A warm phase of $T_w \sim 10^4$ K and $n_w \sim 10^{-1} \text{ cm}^{-3}$ was produced at the interface. This vision is partially confirmed by multi-wavelength observations (see, e.g., Heiles 2001), although reality appears more complex, suggesting the presence of at least 5 different phases.

This picture is challenged by the results of many simulation programs, aimed to the numerical modeling of the ISM (see, e.g., Mac Low et al. 1998; Ostriker, Gammie & Stone 1999; Avila-Reese & Vazquez-Semadeni 2001; Kritsuk & Norman 2002; see Mac Low 2003 and Vazquez-Semadeni 2002 for reviews). In this context the ISM is dominated by compressible, supersonic, MHD turbulence. These groups are still struggling to tame the full complexity of the problem, so that these simulations are not directly aimed to or easily usable by modeling of galaxy formation. For our purposes it is worth mentioning some results. The distributions of temperature and density of the simulated gas particles show a wide range of values without any strong multimodality, but some broad peaks are anyway present. The distribution of pressure shows a much more limited range of values. Structures defined as overdensities are not static clouds but transient features of an overall fractal distribu-

tion (which is consistent with observations, see Chappell & Scalo 2001) that do not last more than a sound crossing time, unless they are gravitationally bound. Thus, the “classical” picture of the ISM is not validated, but a model with multiple phases in rough pressure equilibrium can still be used, though with care, as a useful first-order approximation, able to catch some significant elements of the dynamics of the ISM.

The motivation for the present work is to investigate the kind of physical processes that arise in galaxy formation, in order to provide a grid of solutions for the behaviour of feedback in a wide range of realistic cases, to be used in simulations or semi-analytic models of galaxy formation. We restrict to a two-phase medium in pressure equilibrium, composed by cold clouds embedded in a diffuse hot phase. The dynamics of the ISM is at present assumed to depend only on its “local” properties, leaving thus out “large scale” events like differential rotation, spiral arms, mergers, galactic winds and so on. These events will be introduced once the global characteristics of the galaxy are specified.

This paper is the first of a series aimed to modeling feedback in galaxy formation. It presents a minimal feedback model with its main properties and results. Preliminary results were presented by Monaco (2002; 2003). An upcoming paper will focus on the destruction of collapsing, star-forming clouds (Monaco 2004, hereafter paper II).

The paper is organized as follows. Section 2 describes the physical ingredients of the model, Section 3 introduces the system of equations used, Section 4 the main solutions. Section 5 is devoted to a discussion of the results, and Section 6 gives the conclusions. Finally, three appendices give a list of frequently used symbols, a determination of the time scales of coagulation of cold clouds and a study of the fate of SBs in the n_h - L_{38} plane.

2 FEEDBACK BY STEPS

Feedback is assumed to take place through a chain of processes:

- (i) The densities and filling factors of the two phases are determined by pressure equilibrium.
- (ii) The cooled or infalled gas fragments into clouds with a given mass spectrum; this is truncated at low masses (which are easily destroyed) and at high masses (which continually collapse).
- (iii) Collapse is triggered in clouds larger than the Jeans mass; we use a criterion valid for non-spherical clouds.
- (iv) Collapsing clouds are continually created by coagulation.
- (v) Stars form in collapsing clouds. Self-regulation of star formation by HII regions destroys the clouds before most SNe explode.
- (vi) SN remnants (hereafter SNRs) soon percolate into a SB, which sweeps the ISM. SBs heat the gas whenever they are in the adiabatic stage, i.e. when the interior gas has not had time to cool, while they collapse (and thus cool) the hot phase into a thin cold shell whenever they get into the so-called snowplow stage.
- (vii) SBs stop sweeping or collapsing the hot phase when they remain pressure-confined or overtake the typical vertical scale-height of the system (blow-out).

In the following we describe these steps in detail. All distances are given in pc, masses in M_\odot , times in yr, temperatures in K, gas densities in cm^{-3} , average densities in $M_\odot \text{ pc}^{-3}$, surface densities in $M_\odot \text{ pc}^{-2}$, energies in 10^{51} erg , mechanical luminosities in $10^{38} \text{ erg s}^{-1}$, mass flows in $M_\odot \text{ yr}^{-1}$, energy flows in 10^{51} erg/yr . Pressures are divided by the Boltzmann constant k and given in K cm^{-3} .

2.1 Pressure equilibrium

Let's consider a volume V filled with a two-phase medium, with temperatures of hot and cold phases T_h and T_c and densities n_h and n_c . The volume is assumed to be large enough to contain many star-forming clouds. An external halo acts as a reservoir of gas, which continually replenishes the cold component¹. Stars form from the cold gas. The four components (cold and hot phases, stars and the external halo) have masses M_{cold} , M_{hot} , M_\star and M_{halo} . The total mass of the system is fixed to M_{tot} . The temperature of the cold gas is kept fixed to 100 K, i.e. roughly the position where the cooling function of the gas drops, so that further cooling is inhibited unless the cloud collapses and its density gets very high. Let μ_h and μ_c be the mean molecular weights of the two phases, f_h and f_c their filling factors ($f_h + f_c = 1$), $\bar{\rho}_h = M_{\text{hot}}/V$ and $\bar{\rho}_c = M_{\text{cold}}/V$ their average densities and $F_h = M_{\text{hot}}/(M_{\text{cold}} + M_{\text{hot}})$ the fraction of hot gas. Pressure equilibrium implies:

$$n_h T_h = n_c T_c. \quad (1)$$

From this we obtain:

$$f_c = \frac{1}{1 + \frac{F_h}{1-F_h} \frac{\mu_c}{\mu_h} \frac{T_h}{T_c}}, \quad (2)$$

and of course $f_h = 1 - f_c$, $n_h = \bar{\rho}_h/f_h\mu_h m_p$ and $n_c = \bar{\rho}_c/f_c\mu_c m_p$ (where m_p is the proton mass). Finally, the dependence of the μ_h and μ_c molecular weights on metallicity is taken into account.

2.2 Fragmentation of the cold phase

It is assumed that the cold phase fragments into clouds with a given mass spectrum. As commented in the introduction, according to the turbulent picture of the ISM the “clouds” (i.e. peaks of the fractal density fields) are not stable entities but transient features of the medium. We will assume in the following that the self-gravitating clouds are reasonably stable (in the sense that they are not significantly reshuffled by turbulence) within one or two dynamical times and that the continuous reshuffling of the density field does not change the statistics of clouds.

The mass spectrum of the so-defined clouds is assumed to be a power-law:

$$N_{\text{cl}}(m_{\text{cl}})dm_{\text{cl}} = N_0(m_{\text{cl}}/1 \text{ M}_\odot)^{-\alpha_{\text{cl}}} dm_{\text{cl}}, \quad (3)$$

where N_0 is a normalization constant (with dimensions $\text{pc}^{-3} \text{ M}_\odot^{-1}$), fixed by requiring $\bar{\rho}_c = \int N_{\text{cl}} m_{\text{cl}} dm_{\text{cl}}$ (see below),

¹ The halo is assumed, for simplicity, to be completely decoupled from the hot phase, although in realistic situations the two components will interact.

and α_{cl} is a free parameter. This choice is the natural outcome of many different processes, including turbulence. The parameter α_{cl} can be constrained both from theory and observations of the ISM (see, e.g., Solomon et al. 1987), and should vary between 1.5 and 2 (the latter considered as a reference value), at least in self-regulated situations like the Milky Way. Notice that in this way a significant amount of mass is located in high-mass clouds.

To the clouds we associate a typical radius a_{cl} defined simply as $m_{\text{cl}} = 4\pi a_{\text{cl}}^3 \rho_c/3$, or:

$$m_{\text{cl}} = 0.104 \mu_c n_c a_{\text{cl}}^3 \text{ M}_\odot. \quad (4)$$

This does not imply an assumption of sphericity of the clouds.

The mass function of clouds is truncated both at low and high masses. At the high mass end the mass function is truncated by gravitational collapse, because clouds that form stars are quickly destroyed. The upper mass limit m_u will be computed in the next session. At low masses clouds are easily destroyed by a number of possible processes, among which thermo- and photo-evaporation. McKee & Ostriker (1977) set the lower limit to $a_{\text{cl}} = a_l = 0.5 \text{ pc}$. For $\mu_c \sim 1.2$ and $n_c \sim 10 \text{ cm}^{-3}$ this corresponds to $m_l \sim 0.1 \text{ M}_\odot$. We set the lower mass limit to this value. This is surely a rough approximation, as m_l should be self-consistently determined by the dynamics of the system, and is unlikely to be a constant. However, its actual value does not have a strong impact on the results as long as $m_u \gg m_l$, a condition that is verified by most solutions. Nonetheless it is important to set m_l to a non-vanishing value both to avoid divergence in a few calculations (like the normalization of the mass function for $\alpha_{\text{cl}} \geq 2$) and to avoid contributions from clouds that most likely do not exist.

The normalization constant of the mass function is:

$$N_0 (1 \text{ M}_\odot)^{\alpha_{\text{cl}}} = \frac{\bar{\rho}_c}{f(m_u, m_l)}. \quad (5)$$

Here the function $f(m_u, m_l)$ is equal to $(m_u^{-\alpha_{\text{cl}}+2} - m_l^{-\alpha_{\text{cl}}+2})/(-\alpha_{\text{cl}} + 2)$ if $\alpha_{\text{cl}} \neq 2$, otherwise $f(m_u, m_l) = \ln(m_u/m_l)$.

2.3 Critical mass for clouds

Massive clouds are destroyed by gravitational collapse. In absence of magnetic fields and turbulence the threshold mass for collapse is fixed by the Bonnor-Ebert criterion (Bonnor 1956; Ebert 1955), and depends on an external pressure term P_{ext} . If the external pressure is fixed to the thermal one, the criterion is equivalent to the classical Jeans mass. To generalize it to non-spherical clouds, we follow Lombardi & Bertin (2001), who find:

$$m_J \simeq 1.18 \frac{c_{s,c}^4}{\sqrt{G^3 \mu_{\text{shape}}^3 P_{\text{ext}}}} \simeq 20.3 T_c^{3/2} n_c^{-1/2} \mu_c^{-2} \mu_{\text{shape}}^{-3/2} \text{ M}_\odot. \quad (6)$$

Here $c_{s,c}$ is the sound speed of the cold phase, the external pressure is set to the thermal one and the parameter μ_{shape} is defined by the authors as:

$$\mu_{\text{shape}} \equiv 12\pi \left(\frac{3}{4\pi}\right)^{1/3} \frac{V^{4/3}}{S^2} \quad (7)$$

$$\times S^2 \left(\int_{\partial V} |\nabla_{\xi} u(s\mathbf{x})|^{-1} dS \int_{\partial V} |\nabla_{\xi} u(s\mathbf{x})| dS \right)^{-1}.$$

In this equation the integrals are performed on the surface ∂V (of area S) of the volume V of the cloud; the function u is the cloud density normalized to its maximum value $u \equiv \rho/\rho_{\max}$ and s^{-1} is a “Jeans length” defined as $s = \sqrt{4\pi G \rho_{\max}/c_{s,c}^2}$; \mathbf{x} is the space coordinate and $\xi = s\mathbf{x}$. The parameter μ_{shape} is dimensionless, scale invariant (i.e. does not change for similarity transformations) and is always smaller than unity. For a sphere $\mu_{\text{shape}} = 1$, and the Jeans (Bonnor-Ebert) criterion is recovered. In general, collapsing clouds will be non-spherical, and this will correspond to an increase of the threshold mass m_J . We treat μ_{shape} as a free parameter. It can be considered as a product of two terms, μ_1 and μ_2 , given in the first and second lines of Equation 7. Both terms are ≤ 1 and are unity for a sphere; moreover, μ_2 is unity when gravity is negligible. So, a rough estimate can be obtained by considering $\mu_{\text{shape}} \sim \mu_1$.

This quantity is easily computed in the simple case of a rotational ellipsoid with semi-axes a_1 and a_2 (with the third semi-axis $a_3 = a_2$). If $r = a_2/a_1$ is the axial ratio, we find:

$$\mu_{\text{shape}} \simeq \frac{1}{g(r)^2 r^{4/3}}, \quad (8)$$

where $g(r) = 1/2 + \arcsin \sqrt{1-r^2}/2r\sqrt{1-r^2}$ if $r < 1$ and $g(r) = 1/2 + \log[(r+\sqrt{r^2-1})/(r-\sqrt{r^2-1})]/4r\sqrt{r^2-1}$ if $r > 1$. In this case μ_{shape} takes values ~ 0.5 for axial ratios of order 1:5 (in both senses), while it gets to ~ 0.2 for axial ratios 1:10. As this is likely to be an overestimate of the actual value, we consider 0.2 as a reference value for this parameter.

Magnetic fields and turbulence could in principle invalidate the Bonnor-Ebert criterion by providing non-thermal support to the cloud. Recent simulations (see, e.g., Mac Low 2003) have shown that turbulence cannot inhibit the collapse of critical clouds; the Jeans criterion remains valid provided that the quadratic sum of kinetic and sound speeds is used in place of the sound speed itself. For a typical turbulent speed of several km s^{-1} , the Jeans mass would correspond to that relative to a temperature T_c of several 10^3 K. The effect of turbulent motions can thus be roughly implemented by assuming a very small value for μ_{shape} , of order 0.01. Magnetic fields can halt the global collapse of the cloud but not its fragmentation into stars, so their effect on the critical mass for collapse is negligible.

Finally, in cases like the sweeping of a spiral arm or during a merger the Jeans criterion can be changed by explicitly introducing a P_{ext} term. This will correspond to a sudden decrease of the Jeans mass, and then to a burst of star formation.

2.4 Coagulation of cold clouds

Clouds larger than the Jeans mass are continually created by kinetic aggregation (coagulation) of smaller clouds. This is described with the aid of the Smoluchowski equation (von Smoluchowski 1916). In this we follow the approach of Cavaliere, Colafrancesco & Menci (1991; 1992; see also Menci et al. 2002), who used this formalism to describe the kinetic aggregation of dark-matter halos.

The details of the calculations are reported in Appendix B. In brief, the coagulation of clouds is driven by a kernel:

$$K = \bar{\rho}_c \langle \langle \Sigma_{\text{coag}} v_{\text{ap}} \rangle_v \rangle_m. \quad (9)$$

Here Σ_{coag} is the cross-section for interaction and v_{ap} is the approach velocity, while the two averages are done over velocity and mass. Notably, it is assumed that clouds, although transient, are stable for one crossing time $a_{\text{cl}} v_{\text{ap}}$; this is reasonable as v_{ap} is typically larger than the sound speed of the cold phase. Following Saslaw (1985) the cross-section for the coagulation of two clouds (denoted by 1 and 2) is:

$$\Sigma_{\text{coag}} = \pi(a_1 + a_2)^2 \left(1 + 2G \frac{(m_1 + m_2)}{a_1 + a_2} \frac{1}{v_{\text{ap}}^2} \right). \quad (10)$$

The first term corresponds to geometric interactions, the second to resonant ones; this last term is effective when the approach velocity is not much larger than the internal velocity dispersion of the clouds. In most cases considered here the geometrical term results dominant, so we will neglect resonant interactions in the following. Notice that this cross-section is valid for spherical clouds; we do not consider the effect of asphericity here, as it would be a further-order correction with respect to that of the Jeans mass introduced above.

It is shown in Appendix B that the time scale for coagulation is:

$$t_{\text{coag}} = \left(\frac{4\pi}{3} \right)^{2/3} \frac{1}{\pi} \bar{\rho}_c^{-1/3} \frac{\rho_c}{\bar{\rho}_c}^{2/3} \frac{m_J^{1/3}}{\langle v_{\text{ap}} \rangle} \quad (11)$$

The typical mass scale of the mass function, identified with the upper cutoff, grows like $(1+t/3t_{\text{coag}})^3$. For a Maxwellian distribution of velocities with 1D dispersion σ_v we have $\langle v_{\text{ap}} \rangle = 1.30\sigma_v$.

The time at disposal for accretion is the time necessary to a Jeans-mass cloud to be destroyed. This will be related to the dynamical time:

$$t_{\text{dyn}} = \sqrt{\frac{3\pi}{32G\rho_c}} \simeq 5.15 \times 10^7 (\mu_c n_c)^{-1/2} \text{ yr}. \quad (12)$$

As star formation is triggered roughly after t_{dyn} , and early feedback from young stars destroys the cloud in a comparable time (see below), we conservatively allow aggregation to go on for two dynamical times. Thus, the upper mass cutoff is set to:

$$m_u = m_J \left(1 + \frac{2t_{\text{dyn}}}{3t_{\text{coag}}} \right)^3. \quad (13)$$

The mass of the typical collapsing cloud is then:

$$m_{\text{cc}} = \frac{\int_{m_J}^{m_u} m_{\text{cl}} N_{\text{cl}}(m_{\text{cl}}) dm_{\text{cl}}}{\int_{m_J}^{m_u} N_{\text{cl}}(m_{\text{cl}}) dm_{\text{cl}}}, \quad (14)$$

and the fraction of cold gas presently available for star formation is:

$$f_{\text{coll}} = \frac{\int_{m_J}^{m_u} m_{\text{cl}} N_{\text{cl}}(m_{\text{cl}}) dm_{\text{cl}}}{\bar{\rho}_c}. \quad (15)$$

The total number of collapsing clouds is:

$$N_{\text{cc}} = f_{\text{coll}} \frac{M_{\text{cold}}}{m_{\text{cc}}} \quad (16)$$

Coagulation is a physically motivated and reasonable mechanism to explain the growth of cold clouds, but it has never been validated (to the best of our knowledge) by simulations that include MHD turbulence. Besides, it has been proposed that giant molecular clouds form in the converging flows caused by the sweeping of spiral arms (Ballesteros-Paredes, Vazquez-Semadeni & Scalo 1999), a process that cannot be introduced without a proper modeling of the disc.

A consequence of the assumptions done is that cooling alone is not going to produce clouds larger than the Jeans mass; they are produced only by coagulation of smaller clouds. This is contrary to the naive expectancy of a mass function of clouds which is truncated *below* by the Jeans mass in case of a cooling flow, as only fluctuations larger than the Jeans mass can grow. This is not what is observed in the case of thermal instability in turbulent media, where (without thermal conduction and UV heating) structures of all masses are observed down to the resolution limit (see, e.g., Kritsuk & Norman 2002). On the other hand, it is possible that giant clouds, much larger than the Jeans mass, form in the cooling flows that take place at the centres of cosmological halos. This is neglected here, but can be modeled by introducing a further mass scale in the mass function.

2.5 Star formation and early feedback

Collapsing clouds can reach high enough densities to trigger the formation of H₂ and further cool to ~ 10 K. After one dynamical time (Equation 12) star formation starts inside the “molecular” cloud. An important point is that early feedback from massive stars can destroy the collapsed cloud before the bulk of type II SNe has exploded. It has been shown (Franco, Shore & Tenorio-Tagle 1994; Williams & McKee 1997; Matzner 2002) that HII regions are a source of turbulence, and their energy input is sufficient to destroy the star-forming clouds, pre-heating them at $\gtrsim 10^4$ K. A similar role is played by stellar winds, that are typically trapped inside HII regions (McKee, van Buren & Lazareff 1984). Matzner (2000) computed the amount of turbulence driven into the star-forming cloud by expanding HII regions. Under the assumption that the rate of injection of turbulence equates the decay rate estimated from N-body simulations, he predicted that the cloud would be destroyed in $\sim 2 \times 10^7$ yr, i.e. about one dynamical time of the uncollapsed cloud (Equation 12 with $n_c \sim 10$ cm⁻³), with a resulting efficiency of star formation f_* (i.e. the fraction of the cloud that goes into formed stars) of $\sim 5\text{--}10$ per cent. This is in rough agreement with both observations of molecular clouds and estimates from globular clusters ($f_* \sim 1\text{--}10$ per cent; see, e.g., Elmegreen 2000, 2002).

The ability of the energy from SNe to emerge from the destroyed cloud, possibly the most delicate step in the whole chain of feedback events, is addressed in paper II; here we give only a very short summary of the results. When SNe start to explode the cloud is already in the process of being destroyed, so that a significant fraction of mass is in a warm, diffuse phase. SNRs propagating in this dense environment soon radiate their thermal energy (see next section for more details). In this case, the mass internal to the blast collapses into a thin, dense shell that fragments as soon as the blast is confined by kinetic pressure. So, the net effect of the first SNe is that of collapsing again the diffuse material heated

up by the HII regions. After a few SNe, most gas is re-collapsed into cold clouds with a low filling factor, while the diffuse component has such a low density that SNRs emerge from the cloud before cooling. From this point all the energy from SNe is used to drive the SB. In case many tens of SNe explode in a single cloud, most energy (90-95 per cent) is used to drive the SB, while for very small clouds, where only a few SNe explode, the first SN is able to destroy the cloud, losing most of its energy in the process, while the other SNe (if any) will pump energy into the ISM with a likely high efficiency. Eventually, only ~ 10 per cent of the initial cloud is found in diffuse, hot gas with temperature of order 10⁶ K; lower values are expected if the cloud is particularly dense.

For this version of the feedback model we decide to give a minimal, heuristic description of this process, in order to keep the model simpler. Each SN releases $10^{51} E_{51}$ erg in the ISM². We assume that all the energy is available for driving the SB; in case of very small collapsing clouds a lower effective value of E_{51} will be plausible. We assume that a fraction f_{evap} of the cloud is evaporated to a temperature T_{evap} , while the rest (amounting to a fraction $1 - f_* - f_{\text{evap}}$) is re-collapsed into cold clouds. Of course $f_{\text{evap}} + f_* \leq 1$. We use as reference values $E_{51} = 1$, $f_{\text{evap}} = 0.1$ and $T_{\text{evap}} = 10^6$ K, with the warning that in case of very dense clouds f_{evap} will likely be lower (see paper II).

Finally, the contribution of a single collapsing cloud to the global star formation rate is:

$$\dot{m}_{\text{sf}} = f_* \frac{m_{\text{cc}}}{t_{\text{dyn}}} . \quad (17)$$

2.6 Super-bubbles

SNRs associated to massive stars in a star-forming cloud will soon percolate into a single hot bubble. As a consequence, all the SNe exploding in a cloud will drive a single SB into the ISM (see, e.g., Mac Low & McCray 1988).

Stars are formed with a given Initial Mass Function (hereafter IMF) that must be specified. For the model the only information needed is the mass of stars formed for each supernova, $M_{*,\text{sn}}$. We associate one SN to each > 8 M_⊙ star; if the (differential) IMF has a slope $-(\alpha_{\text{imf}} + 1)$ and the lifetime of a star goes like its mass raised to $-\alpha_{\text{life}}$, the rate of SN explosion goes like $t^{(\alpha_{\text{imf}} - \alpha_{\text{life}})/\alpha_{\text{life}}}$. For standard choices of $\alpha_{\text{imf}} = 1.35$ and $\alpha_{\text{life}} \sim 2.5 - 3$ the exponent takes a value of ~ -0.5 . In other words, the rate of SN explosion depends weakly on time, and is approximated as constant. Denoting by t_{life} the difference between the lifetime of an 8 M_⊙ star and that of the largest star, the number of SNe that explode in a collapsing cloud and the resulting rate are:

$$N_{\text{sn}} = f_* \frac{m_{\text{cc}}}{M_{*,\text{sn}}} , \quad (18)$$

$$R_{\text{sn}} = f_* \frac{m_{\text{cc}}}{t_{\text{life}} M_{*,\text{sn}}} . \quad (19)$$

The mechanical luminosity of the SB is then $L_{\text{mech}} = L_{38} \times 10^{38}$ erg s⁻¹, where:

$$L_{38} = \frac{10^{13} R_{\text{sn}} E_{51}}{1 \text{ yr}} . \quad (20)$$

² Observations suggest values of E_{51} in the range 1 to 10.

Adiabatic stage		
Radius	$R_{\text{sb}}^{(\text{ad})}(t)$	$= 81.3 (L_{38}/\mu_{\text{h}} n_{\text{h}})^{1/5} t_6^{3/5} \text{ pc}$
Shock speed	$v_{\text{sb}}^{(\text{ad})}(t)$	$= 47.7 (L_{38}/\mu_{\text{h}} n_{\text{h}})^{1/5} t_6^{-2/5} \text{ km s}^{-1}$
Average temp.	$\bar{T}_{\text{sb}}^{(\text{ad})}(t)$	$= 1.79 \times 10^5 L_{38}^{2/5} \mu_{\text{h}}^{3/5} n_{\text{h}}^{-2/5} t_6^{-4/5} \text{ K}$
Post-shock temp.	$T_{\text{sb}}^{(\text{ad})}(t)$	$= 5.4 \times 10^4 L_{38}^{2/5} \mu_{\text{h}}^{3/5} n_{\text{h}}^{-2/5} t_6^{-4/5} \text{ K}$
Post-shock press.	$P_{\text{sb}}^{(\text{ad})}(t)/k$	$= 2.16 \times 10^5 L_{38}^{2/5} (\mu_{\text{h}} n_{\text{h}})^{3/5} t_6^{-4/5} \text{ K cm}^{-3}$
Cooling time	$t_{\text{cool}}^{(\text{ad})}(t)$	$= 255 L_{38}^{3/5} \mu_{\text{h}}^{9/10} n_{\text{h}}^{-8/5} \zeta_{\text{m}}^{-1} t_6^{-6/5} \text{ yr}$
Swept mass	$M_{\text{sw}}(t)$	$= 5.53 \times 10^4 L_{38}^{3/5} (\mu_{\text{h}} n_{\text{h}})^{2/5} t_6^{9/5} \text{ M}_{\odot}$
Internal mass	$M_{\text{int}}(t)$	$= M_{\text{sw}}$
PDS stage		
Radius	$R_{\text{sb}}^{(\text{pds})}(t)$	$= 70.2 (L_{38}/\mu_{\text{h}} n_{\text{h}})^{1/5} t_6^{3/5} \text{ pc}$
Shock speed	$v_{\text{sb}}^{(\text{pds})}(t)$	$= 41.2 (L_{38}/\mu_{\text{h}} n_{\text{h}})^{1/5} t_6^{-2/5} \text{ km s}^{-1}$
Post-shock press.	$P_{\text{sb}}^{(\text{ad})}(t)/k$	$= 1.60 \times 10^5 L_{38}^{2/5} (\mu_{\text{h}} n_{\text{h}})^{3/5} t_6^{-4/5} \text{ K cm}^{-3}$
Swept mass	$M_{\text{sw}}(t)$	$= 3.56 \times 10^4 L_{38}^{3/5} (\mu_{\text{h}} n_{\text{h}})^{2/5} t_6^{9/5} \text{ M}_{\odot}$
Internal mass	$M_{\text{int}}(t)$	$= M_{\text{sw}} (1 - (t/t_{\text{pds}})^{-3.2})$

Table 1. Main properties of SBs.

In presence of a two-phase medium the SB expands into the more diffuse, more pervasive hot phase; cold clouds will pierce the blast, but this will promptly reform after the cloud has been overtaken (McKee & Ostriker 1977; Ostriker & McKee 1988; Mac Low & McCray 1988).

The evolution of the SB is described following the model of Weaver et al. (1977; see also Ostriker & McKee 1988). In the beginning the SB is adiabatic, because the shocked ISM has not had time to cool. In this case:

$$R_{\text{sb}}^{(\text{ad})}(t) = 81.3 \left(\frac{L_{38}}{\mu_{\text{h}} n_{\text{h}}} \right)^{1/5} t_6^{3/5} \text{ pc}, \quad (21)$$

where $t_6 = t/10^6$ yr. Table 1 reports the main properties of the SB expanding in the hot phase.

In the adiabatic stage the hot phase is shock-heated by the blast. Of the initial energy of the SN, 73.7 per cent is thermal and 26.3 per cent is kinetic. This stage ends when the post-shock mass elements cool, i.e. when $t_{\text{cool}}^{(\text{ad})}(t) = t$. The cooling time is computed as:

$$t_{\text{cool}} = 3kT/n_{\text{h}}\Lambda(T) \quad (22)$$

and is evaluated at $T_{\text{sb}}^{(\text{ad})}$ (given in Table 1) and $4n_{\text{h}}$ (due to the shock jump condition). For the cooling function we use the approximation proposed, e.g., by Cioffi, McKee & Bertschinger (1988):

$$\Lambda = 1.6 \times 10^{-19} \zeta_{\text{m}} T_{\text{h}}^{-1/2}, \quad (23)$$

where $\zeta_{\text{m}} \equiv Z_{\text{hot}}/Z_{\odot}$ is the metallicity of the hot gas in solar units. This formula is relatively accurate in the range $10^5 \leq T_{\text{h}} \leq 10^{6.5}$. A more realistic cooling function would be desirable, but would make analytic estimates unfeasible. The time of shell formation is then:

$$t_{\text{pds}} = 2.33 \times 10^4 L_{38}^{3/11} \mu_{\text{h}}^{9/22} n_{\text{h}}^{-8/11} \zeta_{\text{m}}^{-5/11} \text{ yr} \quad (24)$$

We call R_{pds} the radius of the SB at t_{pds} . After this moment the swept mass collapses into a thin cold shell. This shell acts like a snowplow, making the swept ISM collapse into it. For simplicity the cold clouds are assumed as before to pierce the shell without any effect. Some of the hot gas will anyway remain inside the bubble, pushing the snowplow with

its pressure; this stage is called Pressure Driven Snowplow (PDS). We use the solution of Weaver et al. (1977; see also Castor, McCray & Weaver 1975) that includes thermal conduction at the interface between the gas and the cold shell, a mechanism that releases more hot gas from the shell into the interior. They obtain:

$$R_{\text{sb}}^{(\text{pds})}(t) = 70.2 \left(\frac{L_{38}}{\mu_{\text{h}} n_{\text{h}}} \right)^{1/5} t_6^{3/5} \text{ pc}, \quad (25)$$

Notice that the time dependence is the same as above, due to the presence of an increasing amount of hot interior gas. This gas is however negligible with respect to the swept mass, and is so diluted that further cooling is inhibited. A more standard choice for the evolution of the SB in the PDS stage would be (see, e.g., Koo & McKee 1992) $R_{\text{sb}}^{(\text{pds})} \propto t^{4/7}$; the exponent decreases only by 5 per cent with respect to Weaver et al. (1977). Table 1 reports the main characteristics of the SBs in this stage.

To ease numerical integration we interpolate between the adiabatic and PDS stages assuming that after t_{pds} the blast radius evolves like $R_{\text{sb}} \propto t^{0.2}$ and the velocity like $v_{\text{sb}} \propto t^{-2}$ until the PDS solutions are met.

In the PDS stage, the amount of ISM swept by the SB that is collapsed into the shell is estimated as the fraction of the internal material for which (in the adiabatic solution) $t_{\text{cool}}(r; t) < t$. Assuming a power-law profile for density and temperature of the gas just inside the adiabatic blast, in the pressure-gradient approximation of Ostriker & McKee (1988) we obtain $T \propto (r/R_{\text{sb}})^{0.5}$ and $\rho \propto (r/R_{\text{sb}})^9$. From these relations we obtain that the internal mass (not yet collapsed into the shell) is related to the swept mass as:

$$M_{\text{int}} = M_{\text{sw}}(t/t_{\text{pds}})^{-3.2}. \quad (26)$$

This is valid of course for $t > t_{\text{pds}}$. For simplicity we assume that the thermal energy of the SB is lost at the same rate:

$$E_{\text{sb}}^{(\text{th})} = 0.737 R_{\text{sb}} t (1 - (t/t_{\text{pds}})^{-3.2}), \quad (27)$$

while the kinetic energy is kept at $E_{\text{sb}}^{(\text{kin})} = 0.263 R_{\text{sb}} t$.

The explosion of the last SN marks the exhaustion of energy injection into the SB, so the evolution after this

event should follow that of a SNR. We observe that SBs are stopped by thermal pressure or by blow-out (see below) before exhaustion in virtually all cases, so an accurate modeling of this stage is immaterial. In any case, we assume that after the last SN has exploded the blast always evolves like the adiabatic Sedov solution for a SNR, $R_{\text{sb}} \propto t^{2/5}$.

A note of caution is necessary on the application of these solutions for the evolution of the SB. They are valid if the hot phase is uniform, the cold phase negligible, and if the mass of the “wind” that drives the SB is negligible with respect to the swept mass. This last condition is violated in most actual cases as soon as a significant fraction of the collapsing cloud is evaporated. On the other hand, the other conditions are also violated: the ISM is structured, and events like thermo-evaporation of clouds, dragging of clouds by the internal gas, turbulent and magnetic pressure and cosmic rays are likely to influence significantly the dynamics of the SB. Some of these effects can be modeled analytically (see Ostriker & McKee 1988), but at the cost of more uncertainties and dangerous assumptions. We decide to rely on the simple solutions given above, with the *caveat* that all numbers must be considered as useful order-of-magnitude estimates.

Nonetheless, we have tried to include thermo-evaporation of the cold phase by the expanding SB, so as to quantify the mass flow implied. Following the approach of McKee & Ostriker (1977) and the generalization of Ostriker & McKee (1988) to SBs, we find that the thermo-evaporated ISM is generally much less massive than the evaporated gas from the star-forming cloud, so the inclusion of thermo-evaporation, while introducing further uncertainties, does not affect strongly the results presented here. We will neglect thermo-evaporation in the following.

2.7 The fate of SBs

An SB can end in two ways: (i) being confined by external pressure, (ii) blowing out of the system.

Case (i) takes place at time t_{conf} when the shock speed is equal to the external, thermal one:

$$v_{\text{sb}}(t_{\text{conf}}) = c_{\text{s,h}} = 91.2(T_{\text{h,6}}/\mu_{\text{h}})^{1/2}, \quad (28)$$

where $T_{\text{h,6}} = T_{\text{h}}/10^6$ K. As the blast propagates into the low-density hot phase, kinetic pressure is always negligible. The time and radius at which confinement takes place are given in Table C1 of Appendix C. After confinement, the blast (in the adiabatic stage) dissolves in the hot phase or the shell (in the PDS stage) fragments because of Rayleigh-Taylor instabilities. This allows the hot phase to mix with the interior hot gas. However, as long as $t_{\text{conf}} < t_{\text{life}}$ many SNe explode after confinement. This will correspond to the creation of secondary bubbles; the medium in which they expand will depend on the velocity with which the interior gas mixes with the external one. In the adiabatic confinement case, it is easy to see that secondary bubbles will be confined in the adiabatic stage as well, so all the energy from SNe will be released to the hot phase; in this case feedback is mostly efficient. In case of confinement in the PDS stage, the situation is more complicated. If interior and external hot gas mix very quickly, the secondary bubbles will expand in the same medium and will then create secondary shells, but if mixing is slow the energy of the

remaining SNe will be pumped efficiently into the hot, rarefied internal gas. To address this case we assume that the energy of the SNe exploding after confinement is released to the hot phase either entirely, $f_{\text{pds}}=1$, or by a fraction $f_{\text{pds}}=0.737(1 - (t_{\text{conf}}/t_{\text{pds}})^{-3.2}) + 0.263$, that takes into account that thermal energy is dissipated according to Equation 27. The two cases should bracket the true solution.

Case (ii), the blow-out of the SB, takes place when the SB overtakes the vertical scale-height H_{eff} of the system, defined as (Mac Low & McCray 1988; Koo & McKee 1992):

$$H_{\text{eff}} \equiv \frac{1}{\rho_0} \int_0^{\infty} \rho_{\text{h}}(z) dz, \quad (29)$$

where z is the vertical direction (that for which H_{eff} is minimal) and $\rho_0 = \rho_{\text{h}}(z=0)$. The blow-out condition is obviously $R_{\text{sb}} = H_{\text{eff}}$, and the blow-out time is reported in Table C1. This condition is true if all SBs are centred at $z=0$. Coagulation naturally leads to mass segregation, and this is in line with the observational evidence that molecular clouds show a smaller vertical scale-length than HI. However, typical blowing-out SBs will be away from the mid-plane and will blow out only from one side, with a result that is not vastly different from a bi-polar blow-out. Moreover, off-plane SBs will blow out more easily, and intermediate configurations with mid-plane SBs being pressure-confined and external SBs blowing out will be possible. In order to keep the model as simple as possible we consider only mid-plane SBs; the H_{eff} vertical scale-length will then be understood as the difference between the HI and H₂ scale-lengths

The SB does not stop immediately after blow-out, as the rarefaction wave that follows blow-out must have time to reach the blast traveling in the horizontal direction. We then allow for a sound crossing time before stopping the SB. If α^2 is the mean effective Mach number of the blast (the square ratio between the blast speed and the average internal sound speed) and $R_{\text{sb}}(t) \propto t^{\eta}$, the sound crossing time of an adiabatic bubble is:

$$t_{\text{cross}} = \frac{\alpha}{\eta} t_{\text{bo}}; \quad (30)$$

For adiabatic and PDS blasts, $\alpha^2 = 1.61$ and 1.18 (Ostriker & McKee 1988; Weaver et al. 1977). The final radius $R_{\text{bo'}}$ and time $t_{\text{bo'}}$ ($\equiv t_{\text{bo}} + t_{\text{cross}}$) at blow-out are reported in table C1. Between t_{bo} and $t_{\text{bo'}}$ the SB can get into the PDS stage (if it hasn't yet) or be confined by pressure.

The final time t_{fin} and radius R_{fin} are defined respectively as the smallest between $t_{\text{bo'}}$ and t_{conf} , and between $R_{\text{bo'}}$ and R_{conf} . Appendix C reports a study of the final state of SBs (confinement or blow-out in adiabatic or PDS stage) in the plane defined by the two variables n_{h} and L_{38} .

At blow-out part of the hot interior gas of the SB escapes to the halo. To compute the fraction of hot blown-out gas we adopt the following simple geometrical model (Fig. 1). The ISM swept by a SB of radius R_{fin} blows out from the two polar cups defined by the intersection of the sphere and the two horizontal planes at distance H_{eff} from the centre. The swept gas receives momentum from the blast in the radial direction, so the blowing-out gas is that contained in a double cone with the opening angle θ of the polar cups; we have $\cos \theta = H_{\text{eff}}/R_{\text{fin}}$. Neglecting the ISM contained in the polar cups (that are outside the volume V), the fraction of swept ISM that is blown out is:

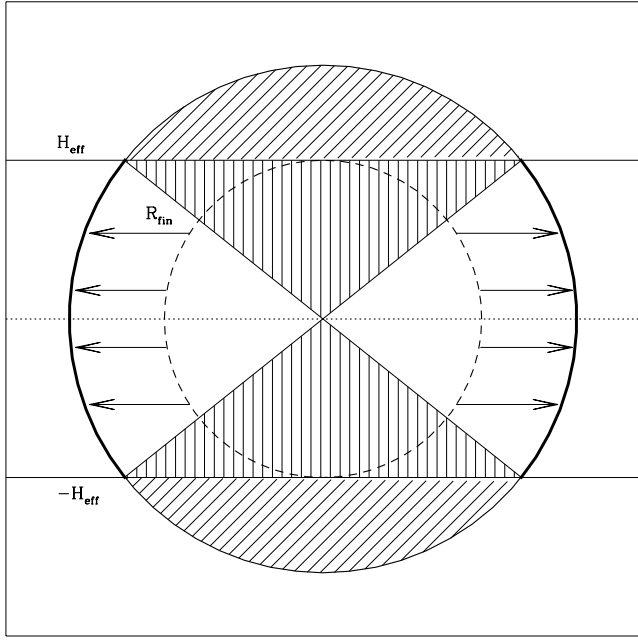


Figure 1. Geometrical model for blow-out. The SB starts blowing out when its radius is equal to H_{eff} , but continues to expand for one sound crossing time, finally reaching the radius R_{fin} . The two polar cups (diagonal-shaded regions), defined by the intersection of the final SB and the two planes at H_{eff} , are assumed to be devoid of matter. All the matter present in the double cone (vertical-shaded regions) with an aperture equal to that of the polar cups receives a radial momentum that allows it to blow-out into the halo.

$$f_{\text{bo}} = \begin{cases} \frac{1}{2} \left[H_{\text{eff}} / R_{\text{fin}} - (H_{\text{eff}} / R_{\text{fin}})^3 \right] & \text{if } R_{\text{fin}} > H_{\text{eff}} \\ 0 & \text{if } R_{\text{fin}} < H_{\text{eff}} \end{cases} \quad (31)$$

This is valid both for adiabatic and PDS blow-out. Consistently, the absence of ISM in the two polar cups is considered when computing the swept mass. With this simple model, that contains no free parameters, the fraction f_{bo} ranges from 0 to ~ 0.2 ; this is roughly consistent with Mac Low & McCray (1988) and Mac Low, McCray & Norman (1989), who report that most of the internal hot gas remains in the disc. It is anyway interesting to allow for higher f_{bo} values; this is done by forcing the maximum of Equation 31 to be $f_{\text{bo},\text{max}}$, which is taken as a free parameter.

A note on definitions: in a cosmological context the term blow-out is used for the gas that is expelled from a galactic halo; we use it for the expulsion of gas from the “galaxy”, i.e. from the region where stars and ISM are present, but our blown-out gas is destined by construction to remain in the halo. As already mentioned above, this over-simplification is introduced to avoid modeling of the external halo. As we know temperature, density and escape velocity of the blown-out gas, modeling of galactic winds is readily feasible once the global properties of the hosting dark-matter halo are specified.

The energy of the SNe exploding after $t_{\text{bo}'}$ is assumed to be funneled out into the halo. Nonetheless, the restored mass, responsible for chemical enrichment, is for simplicity blown out with the same efficiency (f_{bo}) as the rest of the mass, leading to a possible underestimate of the metals ejected into the halo. We will see in the following that the

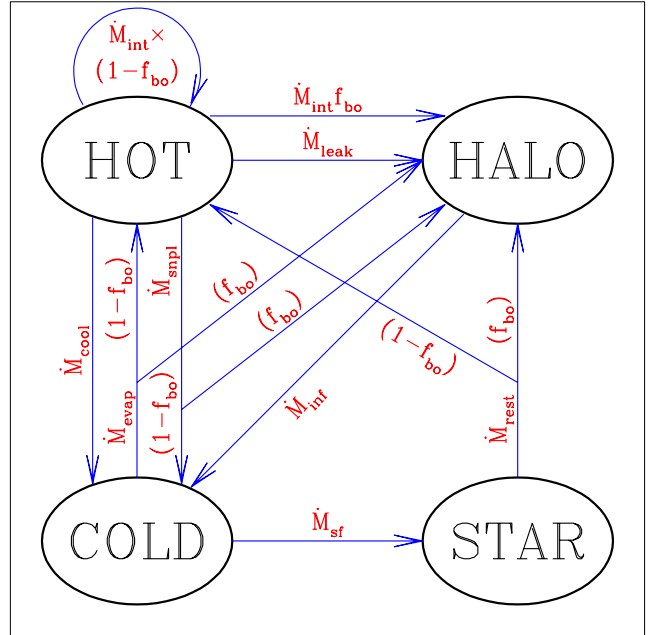


Figure 2. Mass flows between the four components described in the model. Arrows denote the flows connected to infall (\dot{M}_{inf}), star formation (\dot{M}_{sf}), restoration (\dot{M}_{rest}), cooling (\dot{M}_{cool}), evaporation (\dot{M}_{evap}), snowplows (\dot{M}_{snp}), leak-out (\dot{M}_{leak}) and the rate at which the hot phase is engulfed by SBs (\dot{M}_{int}). Blow-out takes mass by a fraction f_{bo} from the internal, evaporation, snowplow and restoration mass flows.

ejection of metals in the halo is anyway rather efficient even with this assumption (see also de Young & Gallagher 1990; Ferrara & Tolstoj 2000). We leave a refinement on this point to further work.

The porosity Q_{sb} of the SBs is defined as the fraction of volume occupied by expanding blasts. This is a very important quantity, as when it is unity it indicates that the blasts percolate the volume and create a super-SB. The computation of Q_{sb} depends on the time at which SBs stop to expand into the ISM. In case of blow-out the blast halts at $t_{\text{bo}'}$ and the energy of further SNe is funneled out of the volume V into the halo. On the contrary, in case of confinement secondary blasts form after t_{fin} , whose energy is still injected into the ISM. To take this into account we compute Q_{sb} as:

$$Q_{\text{sb}} = \frac{N_{\text{cc}}}{t_{\text{dyn}} V} \frac{4}{3} \pi \int_0^{t_{\text{poro}}} R_{\text{sb}}^3(t) dt. \quad (32)$$

where $t_{\text{poro}} = t_{\text{fin}}$ in case of blow-out, or t_{life} in case of confinement; in the latter case R_{sb} is kept constant to R_{fin} after t_{fin} . Regarding the adiabatic blow-out regime, it is clear that if SBs remain identifiable after t_{poro} , then a value of Q_{sb} inferred from observations will be higher than that given by Equation 32. However, recognizable bubbles do not play the same dynamical role as expanding blasts.

3 THE SYSTEM OF EQUATIONS

3.1 Mass flows

Fig. 2 shows all the mass flows between the four components that are taken into account in this model.

Cold gas is continually infalling from the halo. This is modeled simply as follows:

$$\dot{M}_{\text{inf}} = \frac{M_{\text{halo}}}{t_{\text{inf}}}, \quad (33)$$

where t_{inf} is a parameter of the system.

The hot phase cools at the rate t_{cool} ; if it were completely homogeneous it would remain globally hot. In realistic cases the hot phase will show a rather broad range of densities and local cooling times, so that a fraction of the gas will be able to cool to low temperature. A modeling of this fraction would require detailed knowledge of the density distribution of the hot phase; we prefer to leave it as a free parameter, f_{cool} , with 0.1 as a tentative reference value. The cooling mass flux is then:

$$\dot{M}_{\text{cool}} = f_{\text{cool}} \frac{M_{\text{hot}}}{t_{\text{cool}}}, \quad (34)$$

where $t_{\text{cool}}(T_h)$ is computed from Equation 22 and with the simple cooling function given by Equation 23.

While the cold phase is easily confined by a modest gravitational well, the hot phase is generally able to leak out of the volume V to the halo. The time scale connected to this leak-out is:

$$t_{\text{leak}} = \sqrt{3/d} \frac{H_{\text{eff}}}{c_{s,h}}, \quad (35)$$

where $c_{s,h}$ is the sound speed of the hot phase and d is unity if leak-out is on one preferential direction, 3 if it is spherically symmetric. In the following we will consider for simplicity leak-out in one direction; we have verified that the results are not sensitive to the value of d . The mass loss rate is then:

$$\dot{M}_{\text{leak}} = \frac{M_{\text{hot}}}{t_{\text{leak}}}. \quad (36)$$

This term should be revised if some external hot halo gas hampers leak-out.

Cool gas transforms into stars at the rate:

$$\dot{M}_{\text{sf}} = f_{\star} f_{\text{coll}} \frac{M_{\text{cold}}}{t_{\text{dyn}}}. \quad (37)$$

This is easily obtained by multiplying the contribution of a single cloud (Equation 17) by the total number of collapsing clouds N_{cc} (Equation 16). It can be written also as $\dot{M}_{\text{sf}} = M_{\text{cold}}/t_{\text{sf}}$, where

$$t_{\text{sf}} = t_{\text{dyn}}/f_{\star} f_{\text{coll}}. \quad (38)$$

A fraction f_{rest} is instantaneously restored to the hot phase:

$$\dot{M}_{\text{rest}} = f_{\text{rest}} \dot{M}_{\text{sf}}. \quad (39)$$

This flux is responsible for chemical enrichment; we notice that this equation implies instantaneous recycling.

The rate at which the mass of collapsing clouds is evaporated back to the hot phase is:

$$\dot{M}_{\text{evap}} = f_{\text{evap}} f_{\text{coll}} \frac{M_{\text{cold}}}{t_{\text{dyn}}}. \quad (40)$$

It follows that $\dot{M}_{\text{evap}} = f_{\text{evap}} \dot{M}_{\text{sf}}/f_{\star}$.

At the final time t_{fin} each SB has swept a mass $M_{\text{sw}}(t_{\text{fin}})$, of which a part $M_{\text{int}}(t_{\text{fin}})$ (see Table 1 and Equation 26) is in hot internal gas and the rest is in the snowplow. The rate at which the hot phase becomes internal mass of a SB is:

$$\dot{M}_{\text{int}} = N_{\text{cc}} \frac{M_{\text{int}}(t_{\text{fin}})}{t_{\text{dyn}}}, \quad (41)$$

while the rate at which it gets into a snowplow is:

$$\dot{M}_{\text{snpl}} = N_{\text{cc}} \frac{M_{\text{sw}}(t_{\text{fin}}) - M_{\text{int}}(t_{\text{fin}})}{t_{\text{dyn}}}. \quad (42)$$

We recall that a fraction f_{bo} (Equation 31) of the swept material (both hot and cooled) and of the restored and evaporated mass is blown-out to the halo. Defining $\dot{M}_{\text{bo}} = f_{\text{bo}}(\dot{M}_{\text{evap}} + \dot{M}_{\text{rest}} + \dot{M}_{\text{int}} + \dot{M}_{\text{snpl}})$, the system of equations that describes the mass flows is:

$$\begin{cases} \dot{M}_{\text{cold}} &= \dot{M}_{\text{inf}} + \dot{M}_{\text{cool}} - \dot{M}_{\text{sf}} - \dot{M}_{\text{evap}} \\ &\quad + (1 - f_{\text{bo}}) \dot{M}_{\text{snpl}} \\ \dot{M}_{\text{hot}} &= -\dot{M}_{\text{cool}} - \dot{M}_{\text{snpl}} - \dot{M}_{\text{leak}} - f_{\text{bo}} \dot{M}_{\text{int}} \\ &\quad + (1 - f_{\text{bo}})(\dot{M}_{\text{evap}} + \dot{M}_{\text{rest}}) \\ \dot{M}_{\star} &= \dot{M}_{\text{sf}} - \dot{M}_{\text{rest}} \\ \dot{M}_{\text{halo}} &= -\dot{M}_{\text{inf}} + \dot{M}_{\text{leak}} + \dot{M}_{\text{bo}} \end{cases} \quad (43)$$

Mass conservation is guaranteed by the condition $\dot{M}_{\text{hot}} + \dot{M}_{\text{cold}} + \dot{M}_{\star} + \dot{M}_{\text{halo}} = 0$.

3.2 Energy flows

A similar set of equations can be written for the energy flows. Here we concentrate only on the energy E_{hot} of the hot component, that determines T_h . The total energy released by SNe is:

$$\dot{E}_{\text{sn}} = N_{\text{cc}} \frac{E_{51} N_{\text{sn}}}{t_{\text{dyn}}}. \quad (44)$$

The rates of energy loss by cooling, snowplow, blow-out and leak-out are respectively:

$$\dot{E}_{\text{cool}} = \frac{E_{\text{hot}}}{t_{\text{cool}}}, \quad (45)$$

$$\dot{E}_{\text{snpl}} = \dot{M}_{\text{snpl}} T_h \frac{3}{2} \frac{k}{\mu_h m_p}, \quad (46)$$

$$\dot{E}_{\text{bo}} = f_{\text{bo}} \dot{M}_{\text{int}} T_h \frac{3}{2} \frac{k}{\mu_h m_p}, \quad (47)$$

$$\dot{E}_{\text{leak}} = \frac{E_{\text{hot}}}{t_{\text{leak}}}, \quad (48)$$

Regarding the energy budget of the SB (Equation 27), while thermal energy is obviously given to the ISM kinetic energy is transformed into turbulence and then partially thermalized. We have verified that including or excluding kinetic energy from the energy budget does not change appreciably the dynamics of the system. At present we decide to give it to the ISM, more refined modeling of the decay of turbulence will be presented elsewhere.

In the blow-out regime the ISM receives a fraction $(1 - f_{\text{bo}})$ of the energy of the SB (thermal, Equation 27 evaluated at t_{fin} ³, plus kinetic) and of the energy connected to the evaporated mass (that comes from the first SNe exploding in the cloud):

$$\dot{E}_{\text{fb}} = (1 - f_{\text{bo}}) \left(N_{\text{cc}} \frac{E_{\text{sb}}^{(\text{th})} + E_{\text{sb}}^{(\text{kin})}}{t_{\text{dyn}}} + \dot{M}_{\text{evap}} T_{\text{evap}} \frac{3}{2} \frac{k}{\mu_h m_p} \right). \quad (49)$$

³ When t_{fin} is short we force $R_{\text{sn}} t_{\text{fin}}$ to be at least unity.

In the adiabatic confinement case all energy from SNe is given to the ISM:

$$\dot{E}_{\text{fb}} = \dot{E}_{\text{sn}}. \quad (50)$$

In this case the energy of the evaporated cloud is already included in the total SN budget. Finally, in case of PDS confinement the ISM receives the thermal and kinetic energy of the SB. As mentioned in Section 2.7, the energy E_{rest} associated to SNe exploding after t_{fin} is given either by a fraction $f_{\text{pds}}=0.737(1-(t_{\text{fin}}/t_{\text{pds}})^{-3.2})+0.263$ (the case of fast mixing, where secondary bubbles share the same fate as the principal one; see Section 2.6) or entirely, $f_{\text{pds}}=1$ (the case of slow mixing, where the remaining energy is pumped into the rarefied interior of the bubble):

$$\dot{E}_{\text{fb}} = N_{\text{cc}} \frac{1}{t_{\text{dyn}}} (E_{\text{sb}}^{(\text{th})} + E_{\text{sb}}^{(\text{kin})} + f_{\text{pds}} E_{\text{rest}}) \quad (51)$$

Given the uncertainty connected to the modeling of E_{rest} , we consider it worthless to include a detailed treatment of the energy from the evaporated cloud in this case.

The equation for the evolution of E_{hot} is:

$$\dot{E}_{\text{hot}} = -\dot{E}_{\text{cool}} - \dot{E}_{\text{leak}} + \dot{E}_{\text{fb}} - \dot{E}_{\text{bo}} - \dot{E}_{\text{snpl}} \quad (52)$$

The efficiency of feedback f_{E} is defined as the thermal energy gained (or lost) by the ISM (by the hot phase) at the end of the feedback process, divided by the energy injected by SNe. Cooling and leak-out are not directly associated with the action of SBs, while energy losses by blow-out and snowplow act in decreasing the thermal energy of the ISM by depleting the hot phase. We then define f_{E} as:

$$f_{\text{E}} = \frac{\dot{E}_{\text{fb}} - \dot{E}_{\text{bo}} - \dot{E}_{\text{snpl}}}{\dot{E}_{\text{sn}}} \quad (53)$$

It is very important to notice that this quantity is not constrained to be positive: in particular situations the depleting action of blow-outs and snowplows can overtake energy injection; in this case the net effect of SN explosions is a loss of thermal energy more than a gain.

3.3 Metal flows

For each generation of stars a fraction y of the restored mass is composed by new metals that are continually injected into the ISM. We call M_i^Z (where $i=\text{hot, cold, } \star$ or halo) the mass of metals in the various components, and $Z_i = M_i^Z/M_i$ their metallicities. In the instantaneous recycling approximation the system of equations for the metals is:

$$\left\{ \begin{array}{l} \dot{M}_{\text{hot}}^Z = -Z_{\text{hot}}(\dot{M}_{\text{cool}} + \dot{M}_{\text{snpl}} + \dot{M}_{\text{leak}} + f_{\text{bo}}\dot{M}_{\text{int}}) \\ \quad + (1-f_{\text{bo}})[Z_{\text{cold}}\dot{M}_{\text{evap}} + (Z_{\text{cold}}+y)\dot{M}_{\text{rest}}] \\ \dot{M}_{\text{cold}}^Z = Z_{\text{hot}}(\dot{M}_{\text{cool}} + (1-f_{\text{bo}})\dot{M}_{\text{snpl}}) + Z_{\text{halo}}\dot{M}_{\text{inf}} \\ \quad - Z_{\text{cold}}(\dot{M}_{\text{evap}} + \dot{M}_{\text{sf}}) \\ \dot{M}_{\star}^Z = Z_{\text{cold}}(\dot{M}_{\text{sf}} - \dot{M}_{\text{rest}}) \\ \dot{M}_{\text{halo}}^Z = -Z_{\text{halo}}\dot{M}_{\text{inf}} + Z_{\text{hot}}[\dot{M}_{\text{leak}} + f_{\text{bo}}(\dot{M}_{\text{int}} + \dot{M}_{\text{snpl}})] \\ \quad + f_{\text{bo}}[Z_{\text{cold}}\dot{M}_{\text{evap}} + (Z_{\text{cold}}+y)\dot{M}_{\text{rest}}] \end{array} \right. \quad (54)$$

In this case mass is not conserved, the source term being $y\dot{M}_{\text{rest}}$. In these equations it is implicitly assumed that metals are efficiently mixed within each component. This assumption is reasonable for the hot and cold phases, but is clearly wrong for stars. In other words, Z_{\star} is the average metallicity of stars but not that of the last generation, which

contributes to enrichment. As a consequence, we use Z_{cold} for the metallicity of the newborn stars, while the actual distribution of metallicity of stars can easily be obtained by computing the evolution $Z_{\text{cold}}\dot{M}_{\star}$ over time. Mixing of metals within the halo is another delicate assumption; if gas is blown out in form of cold clouds then mixing may be inefficient. A more refined modeling will be required in realistic cases.

3.4 Parameters

It is useful at this point to sum up the parameters introduced in the model. Some of them are connected to the theory of stellar evolution or with the choice of the IMF; we do not regard them as free parameters of the model. In this paper we fix their values as follows: $M_{\star,\text{sn}}=120 \text{ M}_{\odot}$, $f_{\text{rest}}=0.2$, $t_{\text{life}}=2.7 \times 10^7 \text{ yr}$, $y=0.04$.

The following quantities have been introduced in the various steps of the feedback model, and should be regarded as free parameters: α_{cl} , μ_{shape} , E_{51} , f_{\star} , f_{evap} , T_{evap} , f_{cool} . It is worth recalling that f_{evap} and T_{evap} will be determined in paper II, and that T_{evap} plays no role if SBs are pressure-confined. Other parameters are $f_{\text{bo,max}}$, if blow-out is required to be more efficient than the simple geometrical model of Equation 31, and f_{pds} , that regulates the injection of energy after PDS and is relevant only in case of PDS confinement. The parameters T_c and m_l are presently kept constant (we have verified that the solutions do not change much for reasonable changes in these parameters). This parameter space is to be considered as minimal: all the computations presented above are only useful order-of-magnitude estimates, so many quantities could in principle be fine-tuned (with the aid of new parameters) to reproduce, for instance, the results of detailed simulations.

Finally, the total mass M_{tot} , the volume V (or equivalently the total density $\rho_{\text{tot}}=M_{\text{tot}}/V$ or surface density $\Sigma_{\text{tot}}=2H_{\text{eff}}\rho_{\text{tot}}$), the infall time t_{inf} , the vertical scale-height H_{eff} , the velocity dispersion of clouds σ_v and the geometry of leak-out d (fixed to 1 in the following) are the parameters connected to the system in which feedback acts. These parameters are obviously determined by the characteristics of the galaxy; in particular, the galaxy-halo system will never be a “closed box” as naively assumed here, so M_{tot} will not be a constant; ρ_{tot} will be fixed by the gravitational well of the dark-matter halo and the amount of angular momentum retained by the gas; σ_v will be determined by gravitational infall, dissipation and re-acceleration by blasts; H_{eff} will be determined by σ_v and the surface density of the galaxy; t_{inf} will be determined by the cooling and infall times of the dark-matter halo. To avoid the modeling of the galaxy at this stage, we consider for simplicity these parameters as independent. The regions of these parameter space relevant to galaxies will be determined once their large-scale structure is fixed.

4 RESULTS

The system of Equations 43, 52 and 54 has been integrated with a standard Runge-Kutta algorithm with adaptive step-size (Press et al. 1992). The adaptive stepsize is computed considering only the equations for the mass and energy flows.

As mentioned above, the numerical integration is often delicate, especially when the system switches from one regime to another. For this reason it is important to interpolate smoothly between different regimes.

In the following we fix the total mass of the system to $10^{11} M_{\odot}$. All the results can be simply rescaled to any total mass, as long as the mass allows for the presence of at least one collapsing cloud in the volume. The initial conditions are set by putting most gas into the halo, which is both physically reasonable and computationally convenient. The volume V is anyway filled with a small amount of mass in both cold and hot gas and a tiny amount of stars. This sets the system into a physically acceptable transient regime, allowing a smooth integration. We have verified that in general the precise choice of these initial conditions does not influence the result as long as the system starts in a way which is not pathological. Moreover, we set all primordial metallicities to 10^{-4} . We specify the density of the system through the quantity $\rho_{\text{tot}} = M_{\text{tot}}/V$, i.e. the density that the system would have if all the mass were in the volume V and not in the halo. Clearly, the actual density of the ISM will always be smaller than ρ_{tot} . For an easier comparison to astrophysical data, we show results in terms of the surface density $\Sigma_{\text{tot}} = 2\rho_{\text{tot}}H_{\text{eff}}$.

4.1 Feedback regimes for a reference choice of parameters

We choose a reference set of parameters by fixing them to the typical (or tentative) values quoted above in the text: $\alpha_{\text{cl}}=2$, $E_{51}=1$, $f_{\star}=0.1$, $f_{\text{cool}}=0.1$, $\mu_{\text{shape}}=0.2$, $f_{\text{evap}}=0.1$, $T_{\text{evap}}=10^6 K$. For this set of parameters we run the system of equations for a grid of values in the $H_{\text{eff}}-\rho_{\text{tot}}$ (or equivalently $H_{\text{eff}}-\Sigma_{\text{tot}}$) plane, with a time scale of infall $t_{\text{inf}}=10^9$ yr, which is suggested for the Milky Way by galaxy evolution models (see, e.g., Chiappini, Matteucci & Romano 1997), and a velocity dispersion of clouds $\sigma_{\text{v}}=10 \text{ km s}^{-1}$, typical of spiral discs. We stop the integration at three infall times, and check the actual regime of feedback. We have verified that the feedback regime may change with time, but in most cases it does not change from 1 to $3t_{\text{inf}}$.

Fig. 3a reports the regions in the $H_{\text{eff}}-\Sigma_{\text{tot}}$ plane in which various feedback regimes are found. At low Σ_{tot} and H_{eff} values the SBs are able to blow out, and when they do they are always in the adiabatic stage. For increasing H_{eff} it is more and more difficult to blow out, so that SBs are kept confined by the external pressure in the adiabatic stage. The two regimes are roughly separated by the relation shown in the figure:

$$\Sigma_{\text{tot}} = 8 \left(\frac{H_{\text{eff}}}{1000 \text{ pc}} \right)^{-0.8} M_{\odot} \text{ pc}^{-2} \quad (55)$$

At densities lower than this limit by roughly two orders of magnitude the system gets into a critical behaviour, where the hot phase is strongly depleted and the filling factor of the cold phase becomes high. This regime will be described in Section 4.3. At very high surface densities PDS confinement is met; this will be discussed later.

If the vertical scale-length of a disc is set by dynamical equilibrium then $H_{\text{eff}} = \sigma_{\text{v}}^2/\pi G \Sigma_{\text{tot}}$. Galaxy discs will then lie on the continuous lines shown in Fig. 3 for $\sigma_{\text{v}}=5, 10$ and

50 km s^{-1} . Discs with the canonical of $\sigma_{\text{v}}=7 \text{ km s}^{-1}$ will be in the adiabatic blow-out regime, except possibly in the inner parts (where they blend with bulges), while discs with $\sigma_{\text{v}}>10 \text{ km s}^{-1}$ will be in the adiabatic confinement regime. Bright spheroidal galaxies roughly follow a relation of the kind $R_e = 22(M_{\text{tot}}/10^{12} M_{\odot})^{0.6}$ kpc (proposed by Chiosi & Carraro 2002), that can be extrapolated to meet the locus of globular clusters. Identifying the effective radius R_e with H_{eff} , this relation is shown in the $H_{\text{eff}}-\Sigma_{\text{tot}}$ plane as a dashed line. It is clear that feedback in a spheroid will typically be in the adiabatic confinement regime.

4.2 Some examples

We show here examples of the evolution of the system in various regimes. In particular we show the evolution, up to 10 Gyr, of masses and metals of the four components, mass and energy flows, ISM and cloud properties. The evaporation and restoration rates, \dot{M}_{evap} and \dot{M}_{rest} , are not shown in the figures as they are simply proportional to (and smaller than) the star-formation rate \dot{M}_{sf} .

Fig. 4 shows a Milky Way-like system in the adiabatic blow-out regime, with $(H_{\text{eff}}, \rho_{\text{tot}})=(100 \text{ pc}, 0.1 M_{\odot} \text{ pc}^{-3})$ or $\Sigma_{\text{tot}}=20 M_{\odot} \text{ pc}^{-2}$ (it is denoted as MW in Fig. 3). Gas cools but does not transform promptly into stars; in fact, it is continually recycled into collapsing clouds. The final $M_{\text{cold}}/M_{\star}$ ratio is ~ 0.1 . The hot phase regulates to a fraction $F_h \sim 2 \times 10^{-4}$. The halo gas is continually recycled by infall, blow-out and leak-out. Regarding metals, the hot phase is promptly enriched to nearly solar values, followed by the halo gas, which receives the blown-out and leaked-out metals; the final metallicity of the cold gas is solar, those of hot and halo components are 60 per cent higher. The star formation rate \dot{M}_{sf} after a rise of ~ 1 Gyr decreases exponentially from ~ 20 to $\sim 3 M_{\odot} \text{ yr}^{-1}$ in ~ 9 Gyr; the average value of the star-formation rate is $\sim 10 M_{\odot} \text{ yr}^{-1}$. The infall rate \dot{M}_{inf} after ~ 2 Gyr regulates to slightly higher values, while the leak-out rate \dot{M}_{leak} is very similar to the star-formation rate. Notably, leak-out dominates over blow-out, and the cooling term M_{cool} is very low. The energy equation is characterized by the near equality of the two main flows, \dot{E}_{fb} and \dot{E}_{leak} ; this reflects in the very stable value of $T_h \sim 10^6 K$. The ISM is self-regulated and weakly varying over many infall times; its properties are $n_h \sim 10^{-3} \text{ cm}^{-3}$, $n_c \sim 10 \text{ cm}^{-3}$, $P/k \sim 10^3 K \text{ cm}^{-3}$, and change by a factor ~ 5 from 1 to 10 Gyr. The porosity Q_{sb} is low, indicating that active bubbles (i.e. expanding blasts) do not dominate the volume. However, if we assume that SBs are recognizable for a time t_{life} (see Section 2.7), the porosity of “observed” SBs results as high as ~ 1 at a few Gyr and ~ 0.1 at the end of the integration; this implies an apparently bubble-dominated ISM. The filling factor f_c of the cold phase is ~ 0.1 , while the fraction f_{coll} of cold gas in collapsing clouds is slightly lower. The population of collapsing clouds is also rather stable, with masses in a range of roughly a factor of two around $m_{\text{cc}} \sim 10^5 M_{\odot}$. The coagulation time t_{coag} is higher than the dynamical time t_{dyn} by a

⁴ Here we have assumed that the vertical scale-length of the molecular clouds is $H_{\text{eff}}/2$, which amounts to halving H_{eff} to take into account the easier blow-out of SBs that are off the mid-plane; see the discussion in Section 2.7

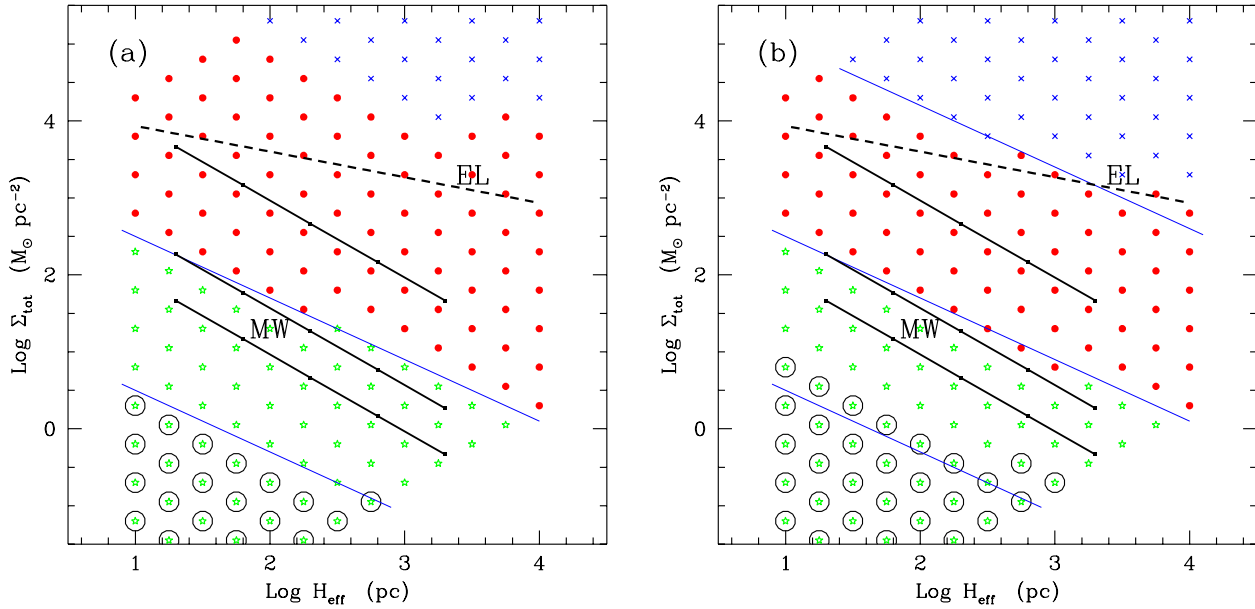


Figure 3. Feedback regimes in the $H_{\text{eff}} - \Sigma_{\text{tot}}$ plane after three infall times. Filled circles denote adiabatic confinement, stars adiabatic blow-out, crosses PDS confinement. Critical cases are marked by circles. Thin lines separate regions with different regimes (see Equation 55), thick continuous lines show the position of spiral discs with (starting from the lowest) $\sigma_v=5, 10$ or 50 km s^{-1} , while the thick dashed line shows the average position of bulges. The labels MW and EL are relative to the examples shown below. Panel (a): reference choice of parameters. Panel (b): $E_{51}=0.3$ and $f_{\text{evap}}=0.05$.

factor of a few, and is $\sim 5 \times 10^7 \text{ yr}$, not very different from the dynamical time of the Milky Way disc. Finally, both the number of clouds and the number of SNe per cloud are high enough to justify the assumptions of the model.

Fig. 5 shows an example of adiabatic confinement (EL) that lies near the elliptical line (Fig. 3), with $(H_{\text{eff}}, \rho_{\text{tot}}) = (3 \text{ kpc}, 0.3 M_{\odot} \text{ pc}^{-3})$ or $\Sigma_{\text{tot}}=1800 M_{\odot} \text{ pc}^{-2}$. In this case, despite of the higher density, gas is consumed more slowly than the previous case, and the final fraction of $M_{\text{cold}}/M_{\star}$ is still ~ 0.5 . The fraction of hot to cold gas is $F_h \sim 10^{-3}$. The pattern of chemical enrichment is similar to the previous cases, although metallicities are lower at the final time (due to the lower amount of gas consumed). Mass flows peak to slightly lower values, and decrease less steeply at later times. Again, star formation regulates nearly to the infall rate after a few infall times, and leak-out is only slightly lower. Blow-out is obviously absent and cooling is again negligible. As before, feedback and leak-out energy flows nearly compensate each other. The ISM is characterized by high pressure ($P/k \sim 10^5 \text{ K cm}^{-3}$), density of both phases ($n_c \sim 10^3 \text{ cm}^{-3}$, $n_h \sim 10^{-2} \text{ cm}^{-3}$), temperature of the hot phase ($T_h \sim 1.5 \times 10^7 \text{ K}$) and a correspondingly lower filling factor of the cold phase ($\sim 2 \times 10^{-3}$). Collapsing clouds are very small ($m_{\text{cc}} \sim 3 \times 10^3 M_{\odot}$), and this is due to the very high density of the cold phase with the consequent low Jeans mass. Besides, the range of collapsing masses is tiny due to the low dynamical time and the consequent inefficient coagulation. This reflects into a low fraction of cold mass in collapsing clouds ($f_{\text{coll}} \sim 10^{-3}$) and a low porosity of active SBs.

This example is useful to understand the change in the behaviour of the system from the adiabatic blow-out to the adiabatic confinement regimes, but clearly a spheroid forms

on shorter time-scales than 1 Gyr, and this leads (within the same physical time) to a consistently more rapid star formation, higher star-formation rates, higher enrichment, higher pressure and densities of ISM, slightly smaller collapsing clouds; however, the temperature of the hot phase and the filling factor and porosity of the cold phase are rather insensitive to the infall time. A similar trend is observed when the density is increased at fixed H_{eff} .

The very low number of SNe per cloud in the adiabatic confinement case highlights a limit of applicability of the model in this case. However, it is easy to check that in the adiabatic confinement regime all terms in the system of Equations (43, 52 and 54) are independent of the actual size of SBs. The thermal energy of the first blast will be radiated away before the SNR manages to destroy the star-forming cloud, so a lower effective value of E_{51} will be reasonably used. The high value of the density of the cold phase highlights another problem. The reason why cold gas is not promptly consumed into stars is that it waits to be included in collapsing clouds. But for such high n_c values the assumption that gravitational collapse is required to trigger the formation of H_2 is probably wrong, and star formation is likely to be spread throughout the cold phase. This can be reproduced simply by forcing f_{coll} to be unity; in this case the evolution of the system becomes trivial, the main mass flows ($M_{\text{sf}}, M_{\text{inf}}, M_{\text{leak}}$ and M_{evap}) become all proportional to each other and decay exponentially over one infall time.

As shown in Appendix C (Fig. C2), to reach the PDS stage at $T_h=10^6 \text{ K}$ it is necessary to have rather high densities n_h and relatively high mechanical luminosities L_{38} ; the constraint tightens considerably at higher temperature. At high densities the Jeans mass is rather low, then L_{38} values

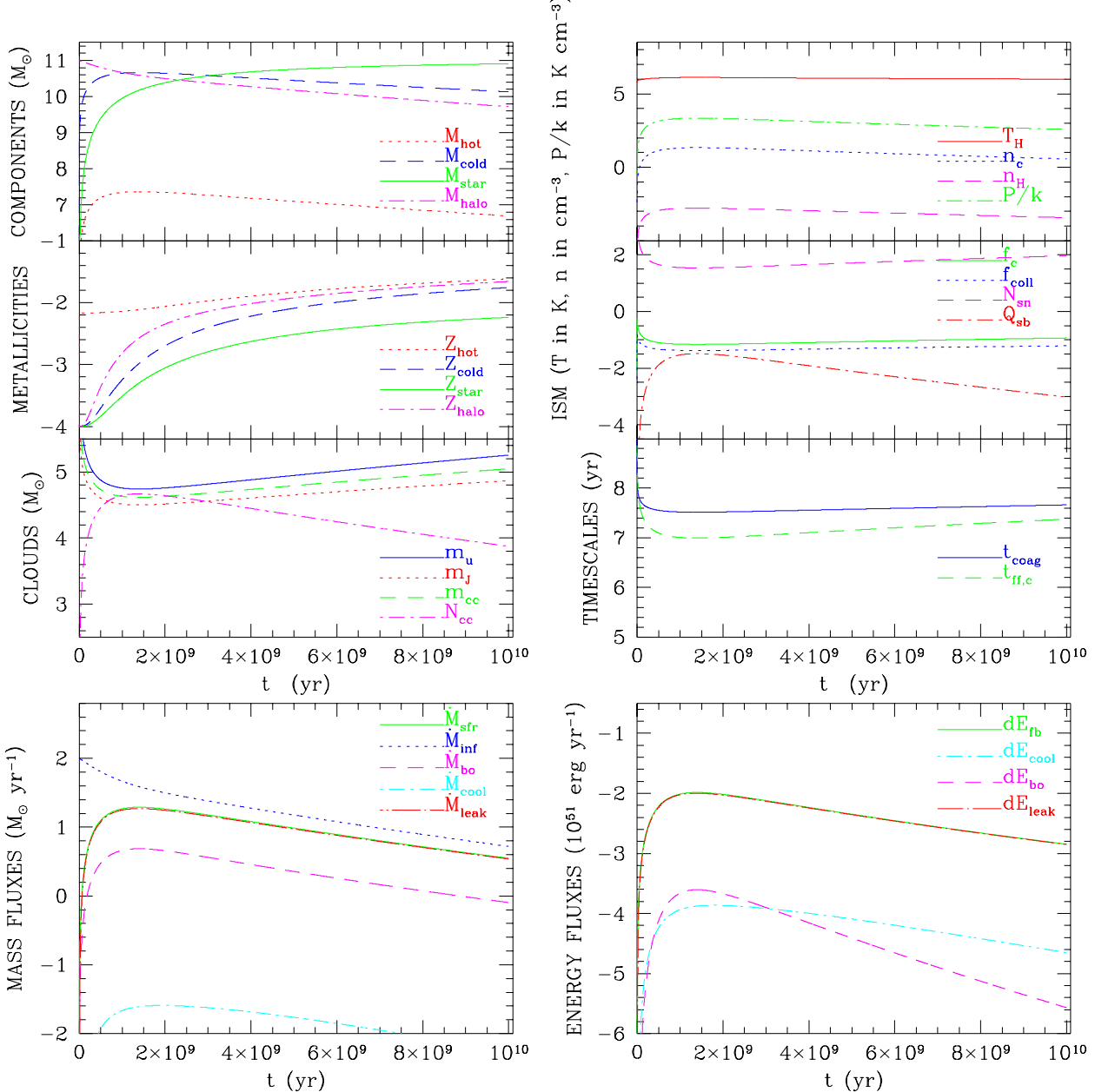


Figure 4. Evolution of the system for the MW adiabatic blow-out example with $(H_{\text{eff}}, \rho_{\text{tot}}) = (100 \text{ pc}, 0.1 M_{\odot} \text{ pc}^{-3})$, $\Sigma_{\text{tot}} = 20 M_{\odot} \text{ pc}^{-2}$. The panels show the main properties of the systems, the quantities and their units are given in the labels. Time is linear, all the quantities given in ordinate are logarithmic. In the lower panels of mass and energy flows, the \dot{M}_{sf} and \dot{M}_{leak} curves and the \dot{E}_{fb} and \dot{E}_{leak} curves are very similar and hardly distinguishable.

are much smaller than unity, so that SBs are mostly kept confined in the adiabatic stage. Higher mechanical luminosities could be achieved by increasing E_{51} , but this implies also a higher T_h . As shown in Table C1, the ratio between t_{pds} and t_{conf} is proportional to $L_{38}^{-5/22} T_h^{5/4}$; as a consequence, the advantage in decreasing L_{38} is over-compensated by the increase in T_h ; as a consequence, PDS confinement is more easily achieved by lowering E_{51} . We recall that for small clouds an effective lower E_{51} value is reasonably obtained

because the thermal energy of the first blast is lost before the blast gets out of the collapsing cloud; moreover, for such dense clouds a lower value of f_{evap} is likely (paper II). Fig. 3b shows the regimes in the $H_{\text{eff}}-\Sigma_{\text{tot}}$ plane for $E_{51}=0.3$ and $f_{\text{evap}}=0.05$; while the limit between adiabatic blow-out and confinement (fig. 3a) is unchanged (and critical cases are found at densities higher by a factor 3), at densities roughly higher than

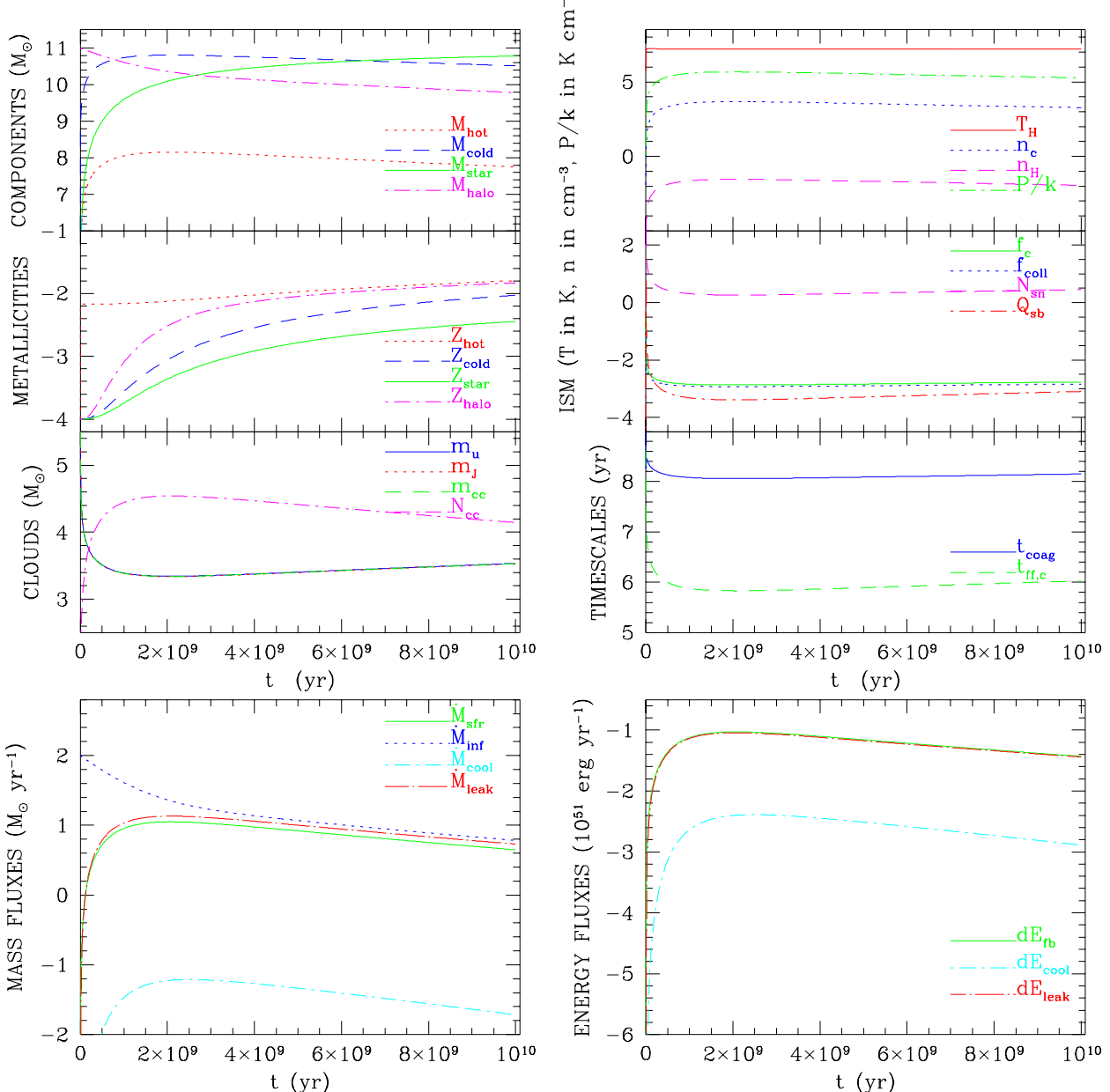


Figure 5. As in Fig. 4, for the EL adiabatic confinement example with $(H_{\text{eff}}, \rho_{\text{tot}}) = (3 \text{ kpc}, 0.3 M_{\odot} \text{ pc}^{-3})$ or $\Sigma_{\text{tot}} = 1800 M_{\odot} \text{ pc}^{-2}$.

$$\Sigma_{\text{tot}} = 2500 (H_{\text{eff}}/1000 \text{ pc})^{-0.8} M_{\odot} \text{ pc}^{-2} \quad (56)$$

PDS confinement is achieved. The reason why it takes place preferentially at high H_{eff} values is because leak-out is inefficient in depleting the hot phase and thus n_h is higher. PDS confinement solutions are found also in Fig. 3a, though at very high surface densities.

The evolution of the system depends sensitively on how the energy of SNe exploding after t_{fin} is given to the ISM. If mixing of hot phase and hot SB gas is slow, energy is pumped efficiently into the hot rarefied medium of the stalled bubble; this corresponds to $f_{\text{pds}} = 1$. Fig. 6 shows again the EL exam-

ple of fig. 5 in this case. PDS confinement starts after a period of ~ 1.5 infall times of adiabatic confinement. Due to the sudden lower injection of energy into the ISM, T_h decreases by nearly an order of magnitude at the start of PDS confinement. This cooling has the effect of increasing t_{pds} ; the system then self-regulates to a configuration in which SBs stop just after PDS, so that the shell never acquires much mass. Pressure and densities are still high, but the filling factor of the cold phase is as high as $\sim 10^{-2}$. As a consequence collapsing clouds are bigger, and f_{coll} is higher. At the onset of PDS confinement the star-formation rate jumps to a

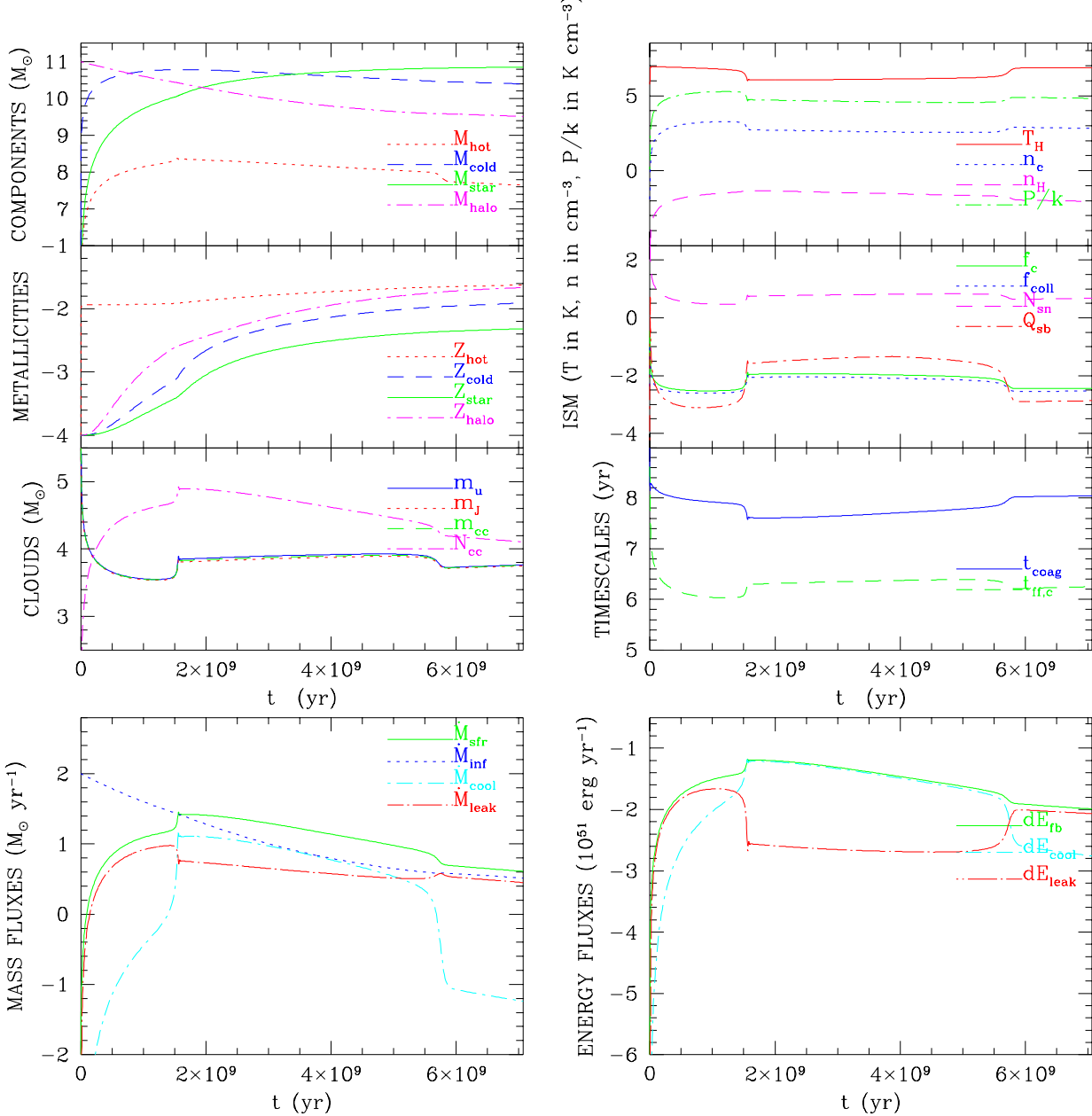


Figure 6. As in Fig. 4, for the EL PDS confinement example ($E_{51}=0.3$, $f_{\text{evap}}=0.05$, $f_{\text{pds}}=1$).

value of $\sim 30 M_\odot \text{ yr}^{-1}$, and then decreases slowly. Due to the lower T_h , the fraction of hot gas is slightly high, $F_h \sim 10^{-3}$. In this regime cooling is more important than leak-out in terms of both mass and energy flows; we have verified that this is always the case for high H_{eff} and Σ_{tot} values. On the other hand, the snowplow flows are small (they are below the range of the energy flux panel), indicating that the most relevant effect of PDS is on the structure of the ISM more than on the mass flows. Notably, the porosity of the SBs increases by more than an order of magnitude. At ~ 6 Gyr

the ISM amounts roughly to 40 per cent of the total mass, and the solution switches back to adiabatic confinement.

For smaller infall times or higher densities the PDS regime is triggered at an earlier time; again we have consistently higher star-formation rates, metallicities, pressure and densities of the ISM, while T_h , f_{coll} and Q_{sb} are hardly affected.

Fig. 7a shows the efficiencies of feedback f_E (Equation 53) in the examples discussed above. Unity values are obtained in the adiabatic confinement regime, while in the PDS confinement example the efficiency is just a few percent

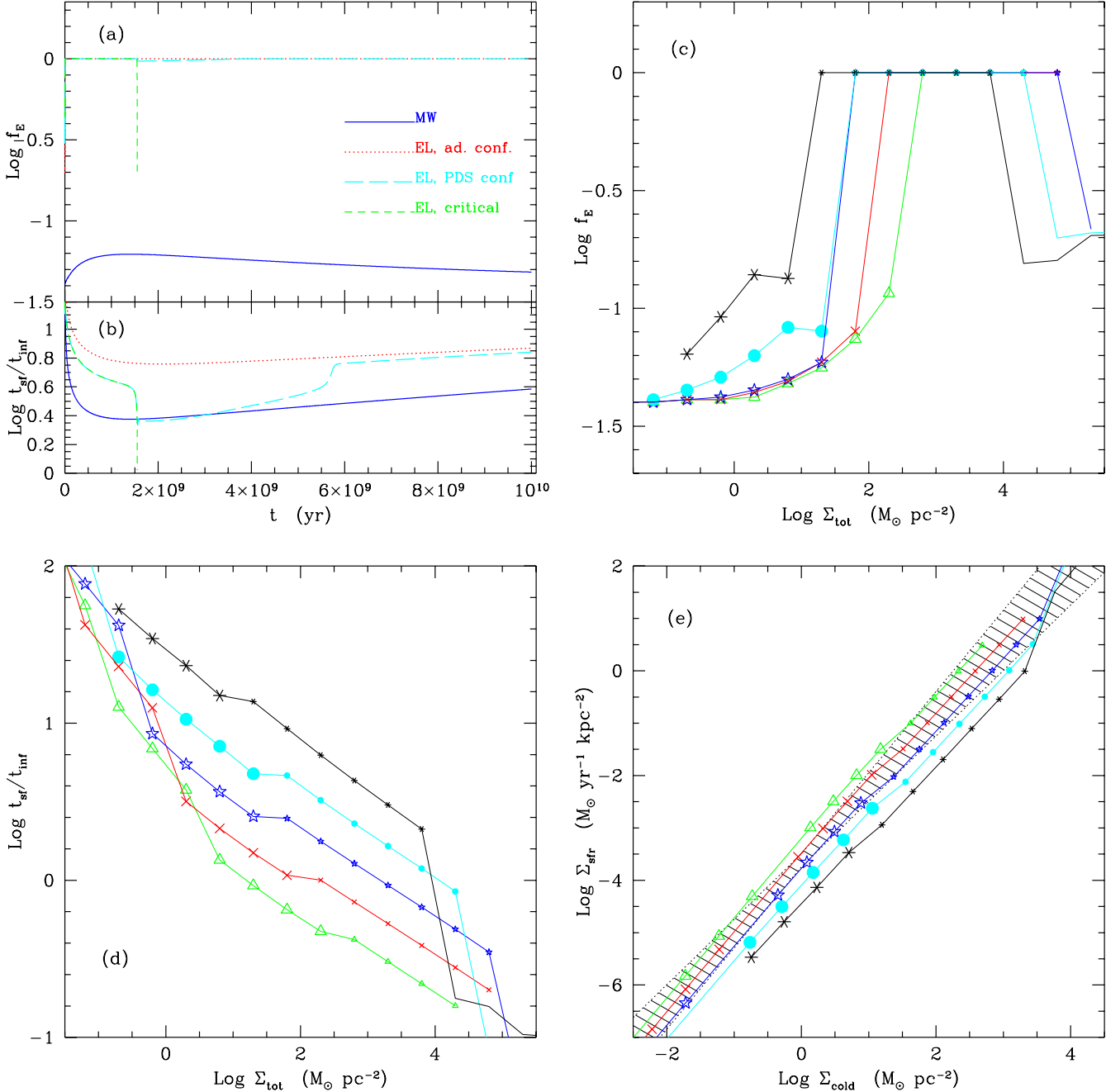


Figure 7. (a) Efficiency of feedback f_E as a function of time for the examples MW and EL with adiabatic or PDS (self-regulated or critical) confinement. (b) Star-formation time-scales (in units of the infall time) for the four cases of panel (a). (c) f_E at three infall times (or at the onset of critical behaviour) for the cases shown in Fig. 3a (with the standard choice of parameters); triangles, crosses, stars, circles and asterisks are relative to $H_{eff}=10, 30, 100, 300$ and 1000 pc; larger points denote the adiabatic blow-out regime. (d) Relation between star-formation time-scale and surface density; symbols as above. (e) Prediction of the Schmidt law versus the observational relation of Kennicutt (1989); symbols as above.

below unity (as apparent in panel (c) smaller values like 0.5 are obtained at higher densities or lower infall times). In the adiabatic blow-out regime most energy is lost to the halo and the efficiency is slightly lower than 0.1. Another way to quantify the efficiency of feedback is through its effect on star formation. We quantify it by the ratio between the star formation time t_{sf} (Equation 38) and the infall time t_{inf} . As

shown in Fig. 7b, a higher efficiency corresponds to a longer star-formation time scale, but the correspondence is only qualitative. For instance, the EL PDS and adiabatic confinement cases have very similar feedback efficiencies but, due to the different ISM structure, star-formation time-scales that differ by more than a factor of two.

It must be kept in mind that f_E refers to the efficiency

with which the energy of SNe is given to the ISM. In the case of adiabatic blow-out, while $\sim 5\text{--}10$ of the energy is given to the ISM, ~ 5 per cent is lost in the destruction of the star-forming cloud (see paper II), and a comparable amount is likely lost in the acceleration of the bubble at blow-out. The remaining ~ 80 per cent of the budget will be available to heat up the halo gas.

Fig. 7c and d show f_E and $t_{\text{sf}}/t_{\text{inf}}$ at three infall times (3 Gyr, or at the final time in critical cases) for the grid of models shown in Fig. 3a. The efficiency of feedback f_E jumps from a value 0.05–0.1 in the adiabatic blow-out cases to 1 in the adiabatic confinement cases and then down to ~ 0.3 in the PDS confinement cases. The star-formation time-scale t_{sf} is roughly fit by a relation:

$$t_{\text{sf}} = 25 t_{\text{inf}} \left(\frac{\Sigma_{\text{tot}}}{1 \text{ M}_\odot \text{ pc}^{-2}} \right)^{-0.3} \left(\frac{H_{\text{eff}}}{1 \text{ kpc}} \right)^{0.5}. \quad (57)$$

Critical and PDS confinement cases fall out of this relation.

In spiral galaxies the star formation rate is well correlated with the amount of cold gas, following the so-called Schmidt (1959) law, quantified by Kennicut (1989) as $\Sigma_{\text{sf}} = (2.5 \pm 0.7) \times 10^{-4} \Sigma_{\text{cold}}^{1.4 \pm 0.15} \text{ M}_\odot \text{ yr}^{-1} \text{ kpc}^{-2}$ (with Σ_{cold} the surface density of cold gas in $\text{M}_\odot \text{ pc}^{-2}$). Fig. 7e shows the predictions of this relation for the same grid of models at 3 Gyr, compared to the Kennicut relation. While the slope is accurately reproduced, the normalization depends on H_{eff} , and is well reproduced for $H_{\text{eff}} \sim 50\text{--}100$ pc. Bright spirals are known to have roughly constant surface densities and velocity dispersion of clouds, so the average value of H_{eff} is also constant and of order of its value in the solar neighbourhood. So, the predictions of this model satisfy the Schmidt-Kennicut law also in its normalization. We have verified that this agreement holds in a very broad range of cases and at all times. This implies that this is a robust prediction of the model, but cannot be used to fine-tune the parameters. The Schmidt-Kennicut law is naturally obtained if star formation depends on the mass of the cold gas divided by its dynamical time. In our case (Equation 37) the relation is not built-in, due to the presence of the f_{coll} fraction and to the fact that the dynamical time is computed on the actual and not average density of the cold phase. The Schmidt-like law then follows from the approximate constancy of f_{coll} and f_c .

Finally, the Schmidt-Kennicut law is not followed in the external regions of spiral galaxies, where star formation is quenched. This is not predicted by the present model. However, such star-formation edges are usually thought to be an effect of differential rotation or, according to Schaye (2004), of photo-heating by the cosmological UV background. Both processes are not included here, so this disagreement is expected and is not considered as a worry.

4.3 Critical examples

As long as the system of equations described in Section 3 holds, the physical system is self-regulated; as we have seen, equilibrium solutions are found in which the ISM is relatively stable for many infall times. However, there are critical cases where the conditions for the existence of a two-phase medium are violated and the system of equations does not hold any more.

At densities roughly two orders of magnitude lower than

the limit shown by Equation 55 the system gets into a critical regime, where the hot phase is strongly depleted and the filling factor of the cold phase f_c is larger than that of the hot phase f_h , violating the assumption of a cold phase fragmented into well-separated clouds. The cases where this happens are highlighted by a circle in Fig. 3. The reason for this behaviour is simple: at such low densities star formation is very weak, while for a thin structure leak-out is strong, so the hot phase cannot be sustained. This is not very informative, as such low-density thin systems, if they exist, would be kept ionized by the cosmological UV background, so star formation would never start.

A similar phenomenon happens in other cases for different reasonable choices of the parameters, with the difference that high values of f_c are obtained not from the start but after some time. If we allow $f_{\text{bo,max}}$ to be as large as 0.8, the blow-out mass flux is much stronger and dominates over leak-out. For $\Sigma_{\text{tot}} \sim 200\text{--}1000 \text{ M}_\odot \text{ pc}^{-2}$, when H_{eff} increases above ~ 1 kpc the system does not go into the adiabatic confinement regime; SBs get bigger and blow-out gets stronger, severely depleting the hot phase. Pressure and densities are low, collapsing clouds are very massive (up to 10^6 M_\odot) and Q_{sb} is high (even higher than unity). The hot phase is so strongly depleted that eventually, after roughly one infall time, $f_h < f_c$. When the cold phase percolates the volume, the most likely outcome is collapse (the total mass of cold gas is surely larger than m_J) and a sudden burst of star formation without any obvious external trigger. In other words, star formation would switch from a “candle”-like to a “bomb”-like solution. For a dynamical time $t_{\text{dyn}} \sim 5 \times 10^7 \text{ yr}$ (in this case $n_c \sim 1 \text{ cm}^{-3}$) and for an efficiency $f_* \sim 0.1$, 10^{10} M_\odot of cold gas would give rise to a starburst of tens of $\text{M}_\odot \text{ yr}^{-1}$.

Another example of critical behaviour is found when a high-density system goes into the PDS confinement regime (see the previous subsection). If the mixing of hot phase and hot internal gas is fast, then more thermal energy is lost to radiation and $f_{\text{pds}} = 0.737(1 - (t_{\text{fin}}/t_{\text{pds}})^{-3.2}) + 0.263$ (Equation 51). In this case, when PDS confinement is triggered T_h decreases dramatically, and the hot phase collapses in a very short time. Fig. 8 shows the evolution of the same example of Fig. 6 for this choice of f_{pds} . The collapse of the hot phase takes place at the start of PDS, after 1.5 infall times (1.5 Gyr). The cold gas will be promptly consumed into stars; for a conservative value of $f_* = 0.1$ this will give rise to a brief star formation episode with \dot{M}_{sf} in excess of $100 \text{ M}_\odot \text{ yr}^{-1}$. The porosity of SBs takes values larger than unity at PDS, indicating the formation of a unique super-SB that will plausibly remove all the ISM not consumed by star formation. This super-wind will interact with the external halo gas, so that further infall will be halted for some time.

The actuality of these critical solutions is uncertain, as they could be due to some of the simplifications introduced. In low-density cases, magnetic fields or turbulence could keep the cold medium fragmented even in the presence of low thermal pressure, or the hot phase could be replenished by mass flows neglected here, while in high-density cases the existence of critical solutions depends sensitively on the way the energy of SNe exploding after the SB stalls is given to the ISM. In any case, the idea of a critical ISM deserves further investigations.

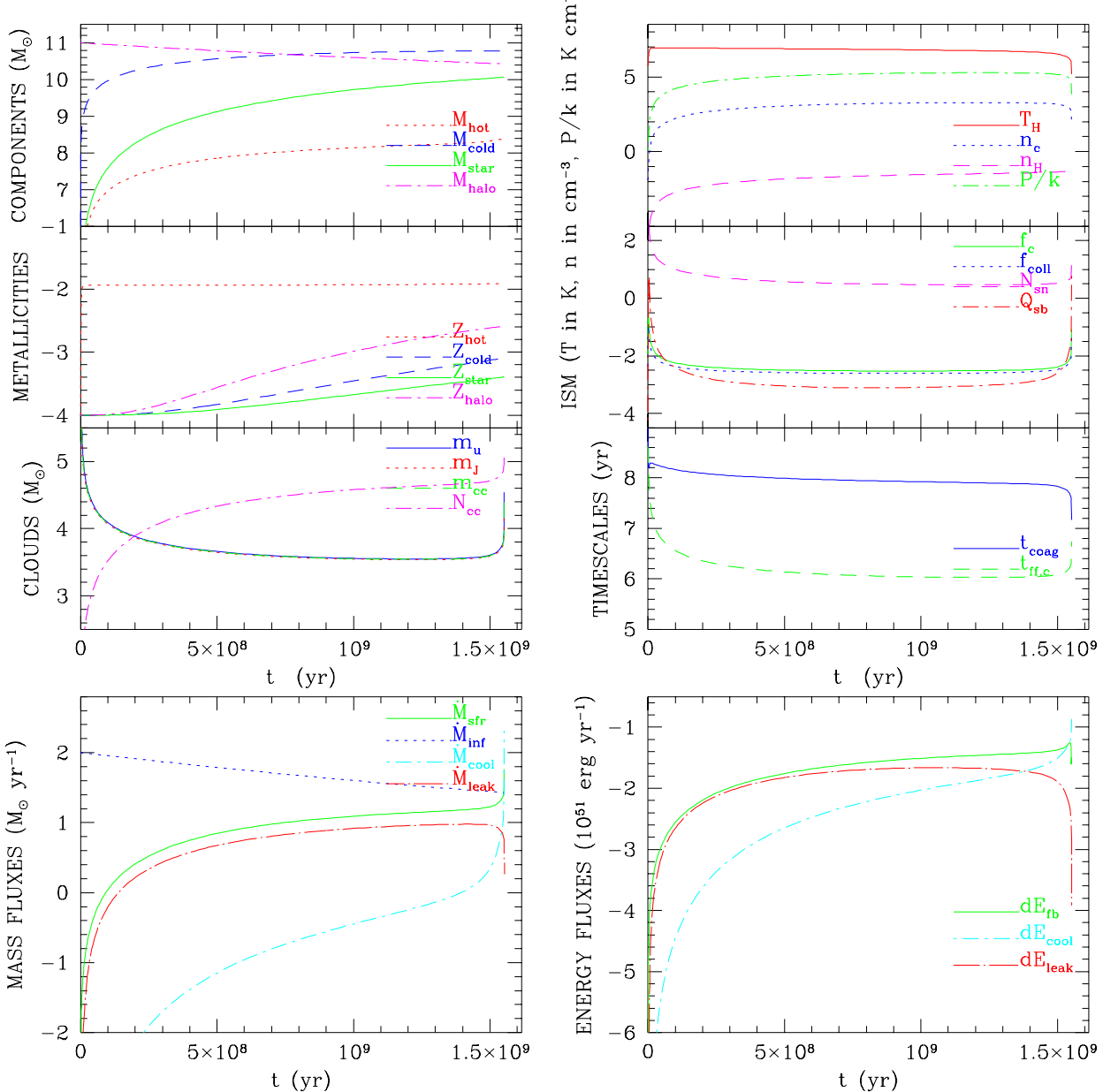


Figure 8. As in Fig. 6, but with $f_{\text{pds}} = 0.737(1 - (t_{\text{fin}}/t_{\text{pds}})^{-3.2}) + 0.263$.

4.4 Probing the parameter space

In the following we give a brief account of the effects of changing the various parameters within reasonable limits.

The value of σ_v enters formally in the coagulation time (Equation 11), so a hypothetical increase of σ_v at fixed H_{eff} and Σ_{tot} reflects in a decrease of the coagulation time, and an increase of the largest collapsing mass m_u (Equation 13), with a corresponding increase of the collapsing mass m_{cc} (Equation 14), the fraction of cold gas available for collapse f_{coll} (Equation 15) and a resulting higher (and more quickly decreasing) star formation rate (Equation 37). However, the

collapsing mass m_{cc} is set mostly by the Jeans mass, so the results are rather insensitive to the precise value of σ_v . Of course, in real systems a change in σ_v would imply a change in H_{eff} or Σ_{tot} , with the known effects.

Decreasing t_{inf} results in a correspondingly stronger star formation rate, and in a faster recycle of materials, while increasing it has an opposite effect. Again, the feedback regimes do not change much; with fast infall adiabatic confinement is reached at slightly lower densities.

The effect of decreasing α_{cl} is that of moving mass to the high-mass end of the mass function of cloud, and thus

to increase f_{coll} and \dot{M}_{sf} . An increase of the star-formation rate is obtained also by increasing f_{\star} (Equation 37). However, the two cases are rather different in terms of cold gas: with low f_{\star} and α_{cl} values the cold gas is reprocessed by collapse many times, while with high values it is locked in the small clouds until it is processed by star formation. On the feedback regimes, lowering α_{cl} or f_{\star} has the effect of moving the limit for adiabatic blow-out at lower densities, especially at low H_{eff} values, and vice-versa for an increase of α_{cl} or f_{\star} .

An increase of μ_{shape} to unity lowers the Jeans mass (Equation 6), making blow-out more difficult; also, a lower number of SNe per cloud in the adiabatic confinement case is obtained. The opposite happens for a decrease of μ_{shape} , which is justified if collapsing clouds are supported by kinetic or magnetic pressure; for $\mu_{\text{shape}}=0.05$ adiabatic blow-out is easily reached at densities higher by an order of magnitude than the limit given in Equation 55.

As mentioned above, a low value of E_{51} leads to lower T_{h} , lower pressure and a corresponding increase of the Jeans mass; moreover, PDS confinement is found at high H_{eff} and Σ_{tot} values. Increasing E_{51} leads to an increase of T_{h} , that for $E_{51}=10$ can reach extremely high and unlikely values. The limit between the adiabatic blow-out and confinement regimes does not depend much on E_{51} .

As cooling is a relatively modest mass flux, the results do not depend sensitively on the parameter f_{cool} , with the exception that PDS confinement is reached more easily for $E_{51}=1$ whenever $f_{\text{cool}} \ll 1$.

The parameters f_{evap} and T_{evap} mostly affect the adiabatic blow-out regime; in particular T_{evap} influences strongly the resulting T_{h} . A low value of f_{evap} increases the number of critical blow-out cases, until T_{evap} is increased to compensate for the lack of evaporated mass. If both parameters are increased, the limit for adiabatic blow-out lowers. Finally, with a high f_{evap} value PDS confinement is reached at high densities even for $E_{51}=1$.

4.5 On the vertical scale-height of the hot phase

The assumption of one single vertical scale-height for both cold and hot phases is clearly over-simplistic; it can be relaxed by assuming two different scale-heights, but in absence of further constraints this new degree of freedom would not contribute significantly to the understanding of the problem. Anyway, the assumption is sensible as the hot gas is continually replenished within H_{eff} . The hot gas that leaks out into the halo is likely to settle in a low-density layer that surrounds the galaxy. Such layer is observed in the Milky Way (see, e.g., Jenkins 2002) as well as in nearby galaxies (see, e.g., Ferguson et al. 1995; Fraternali et al. 2002). The presence of a sufficiently steep decreasing density gradient at H_{eff} is enough to guarantee that this layer does not hamper the blow-out of SBs. Indeed, the interaction of blown-out gas and such a layer could be at the origin of the observed correlation of X-ray and H α fluxes in nearby starburst galaxies (Strickland et al. 2002).

We can estimate the thickness of this layer, that we call H_{h} , as follows. We assume that the expansion of the leaked-out gas stops after one cooling time. For a gas in adiabatic expansion we have $n'_{\text{h}} = n_{\text{h}} H_{\text{eff}} / H_{\text{h}}$, $T'_{\text{h}} = T_{\text{h}} (H_{\text{eff}} / H_{\text{h}})^{\gamma-1}$ and $c'_{\text{s,h}} = c_{\text{s,h}} (H_{\text{eff}} / H_{\text{h}})^{(\gamma-1)/2}$, where the prime indicates

the quantities relative to the gas layer and γ is the adiabatic index, assumed to be 5/3. It is easy to see that, for the cooling function given in Equation 23 the cooling time is constant with H_{h} . The equilibrium value of H_{h} will satisfy the condition $t_{\text{cool}} = H_{\text{h}} / c'_{\text{s,h}}$. To compute it, we take into account that there is continuous injection of hot gas with a roughly constant rate within one cooling time. We obtain:

$$H_{\text{h}} = \frac{4}{7} H_{\text{eff}} \left(\frac{t_{\text{cool}} c_{\text{s,h}}}{H_{\text{eff}}} \right)^{3/4}. \quad (58)$$

For the adiabatic blow-out case of Fig. 4 we obtain $H_{\text{h}} \sim 2$ kpc. This will be an overestimate, as gravity is likely to be important at such distances from the centre of the galaxy.

Alternatively the expansion of the hot phase could progress in such a way not to create a steep density gradient. In this case the hot phase would be contained in a layer of thickness H_{h} and nearly constant density. Exploiting Equation 58, it is possible to include the dynamical evolution of such a layer in the system of equations; in this case leak-out would not be considered as the hot phase formally never gets back to the halo. As a result, the hot gas produced by SNe pushes the layer to high enough H_{h} values that adiabatic confinement is always achieved. The predictions of this version of the model are found in striking disagreement with observations in the Milky Way-like case (see next section), so the possibility of a hot gas layer with a roughly constant density will not be further considered.

5 DISCUSSION

5.1 The Milky Way

To highlight the predictive power of the model, we compare the results of the Milky Way-like adiabatic blow-out case shown in Fig. 4 with available observational evidence. It is useful to stress that no accurate modeling or fine-tuning of parameters is attempted at this stage, so an order-of-magnitude agreement is considered a success. The predictions of n_{h} ($\sim 10^{-3} \text{ cm}^{-3}$), n_{c} ($\sim 10 \text{ cm}^{-3}$) and T_{h} ($\sim 3 \times 10^6 \text{ K}$) are in broad agreement with the ISM of the Milky Way. Thermal pressure ($\sim 10^3 \text{ K cm}^{-3}$) is in line with observations, but is an order of magnitude lower than the observed total pressure, which is dominated by turbulent and magnetic contributions. The mass ratio of cold gas to stars (~ 0.1) is correctly reproduced after 10 Gyr.

The star formation rate \dot{M}_{sf} is slowly decreasing in time, with a ratio of average to final rates of ~ 3 . This is roughly consistent with the results of the chemical evolution model of Chiappini et al. (1997).

Both the average value and the range of the masses of collapsing clouds are smaller than those observed for molecular clouds, that can be as large as $m_{\text{cl}} \gtrsim 10^6 M_{\odot}$. Large collapsing clouds are easily obtained by using a very low value for μ_{shape} , on the ground that kinetic support determines the Jeans mass m_{J} (Section 2.3). The small range of collapsing cloud masses reflects in the low values of f_{coll} , the fraction of cold mass in collapsing clouds; it is predicted to be ~ 5 per cent, at variance to the observed ~ 50 per cent. To obtain higher f_{coll} values it is useful to decrease α_{cl} to the observed value of 1.6, decreasing also f_{\star} to avoid excessive star formation (this is also consistent with observations). However, good f_{coll} values are obtained only by allowing clouds

to coagulate for at least 10 dynamical times. This unrealistic value is not worrisome if we consider the uncertainty connected to the coagulation picture; while the coagulation time, $t_{\text{coag}} \sim 5 \times 10^7$ yr, is coincidentally similar to the time interval between the sweeping of two spiral arms, the formation of molecular clouds in the converging flows of spiral arms (Ballesteros-Paredes, Vazquez-Semadeni & Scalo 1999) could easily be more efficient than random aggregations of clouds, and this could be mimicked by allowing coagulation to work for many dynamical times.

The thickness of the layer of leaked-out hot gas is predicted to be ~ 2 kpc, in rough agreement with the value of ~ 3 kpc estimated for the Milky way by Savage et al. (2000; see also Jenkins 2002). However, this estimate is based on FUSE detection of O VI absorption lines of OB stars; this method is sensitive to temperatures in a narrow range around $\sim 3 \times 10^5$ K. The gas leaking out at $T_h = 10^6$ K has adiabatically cooled to $\sim 1.5 \times 10^5$ K at 2 kpc, while the temperature of $\sim 3 \times 10^5$ K is reached at ~ 0.6 kpc, significantly less than observed. However, this prediction depends sensitively on the parameter T_{evap} , that influences the temperature of the hot phase. If this parameter is increased by a factor of 3 (a reasonable choice according to paper II), the resulting layer is predicted to be 10 kpc thick, reaching a temperature of $\sim 3 \times 10^5$ K at ~ 3 kpc as observed.

With reasonable choices of the parameters, and allowing coagulation to work for 10 dynamical times, it is possible to reproduce all these properties of the Milky Way. The reason why we do not stress this result is because we consider the present model too simple to draw significant conclusions from it. By interfacing this model with an algorithm for disc formation in a cosmological dark-matter halo and including the effect of differential rotation and spiral arms it will be possible to produce accurate predictions for the Milky Way, including galactic fountains, high-velocity clouds, chemical enrichment of the various components, chemical gradients along the disc and so on. By reproducing the observed Milky Way it will be possible to constrain most model parameters by modeling just one galaxy.

5.2 Critical solutions and the triggering of galactic winds

Although a proper modeling of galactic winds requires specifying the properties of the dark-matter halo hosting the galaxy, it is interesting to analyse the cases in which feedback could lead to the removal of a significant quantity of ISM from a galaxy. As removal of gas from a halo with low circular velocity can be achieved even with a single SB (see, e.g., Ferrara & Tolstoy 2000), we will concentrate on bright galaxies. Blow-out leads to the expulsion of matter with a velocity that, in the example of Fig. 4, ranges from ~ 250 km s $^{-1}$ at 1 Gyr to more than 500 km s $^{-1}$ at later times, so if these clouds are not slowed down significantly by the halo gas (e.g. by the layer of leaked-out hot gas) they may escape even from relatively high-mass halos. Anyway, blow-out flows are never very strong, so blow-out is unlikely to lead to massive removal of ISM from a galaxy. Besides, leaked-out gas cools below 10^5 K at ~ 10 kpc, so it will be emitted as a tenuous wind from the low-mass halos, but will be retained by the halo of a bright galaxy. Leaked-out gas is much hotter in the adiabatic confinement regime, so this gas will be able

to escape from moderate-sized halos, but will be retained for instance in big elliptical galaxies. In conclusion, as long as blasts propagate into the hot phase and SBs do not percolate the volume, the removal of mass is inefficient in bright galaxies.

This conclusion changes in the critical cases, where a significant amount of gas accumulated for some time is consumed in a few dynamical times, and when the porosity of SBs gets unity value.

Critical solutions are found at least in three cases: (i) thin, very low- Σ_{tot} systems in the adiabatic blow-out regime, (ii) thick, moderate- Σ_{tot} systems in the adiabatic blow-out regime (in case of very efficient blow-out) and (iii) thick, high- Σ_{tot} systems in the PDS confinement regime (with low E_{51} and low f_{pds}). While case (i) has no astrophysical relevance (such systems would anyway be kept ionized by the cosmological UV background), case (ii) may correspond to some gas-rich dwarf galaxies and case (iii) to high-redshift spheroids.

When these systems become critical, all the cold phase collapses and gives rise to diffuse star formation. For a conservative f_{\star} value of 0.1, we estimated star-formation rates of tens of M_{\odot} yr $^{-1}$ for case (ii) and in excess of $100 M_{\odot}$ yr $^{-1}$ for case (iii). In such big bursts f_{\star} could well take unit values, thus boosting star formation rates even higher; on the other hand, if the transition from the “candle”- to the “bomb”-like regime is not as quick as assumed, star formation rates will be lower. Analogously to what happens in star-forming clouds, the exploding SNe will propagate into the diffuse cold phase, going soon in the PDS stage and then percolating the volume. This will give raise to a unique SB with a very high mechanical luminosity, able to sweep the whole galaxy. This snowplow will eventually blow out of the galaxy and then fragment because of Raileigh-Taylor instabilities. If the momentum of the gas in the fragmented snowplow at this point is sufficient, it will be thrown out of the galaxy.

Percolation of SBs gives a similar effect if it takes place in the PDS confinement (or blow-out) regime; though it has been assumed for simplicity that clouds pierce the snowplow, this is likely true only for the largest and densest clouds, that would likely be star-forming in this case. The effect of a percolation of collapsed shells would be to create a super-SB that sweeps the ISM, pushing part of the gas out of the galaxy in form of cold clouds while the rest is compressed toward the centre of the galaxy. This is found, for instance, in the simulations of primordial galaxies by Mori, Ferrara & Madau (2002); as the physics is the same, their conclusion can be extended to larger, lower-density galaxies, as long as percolation of SBs in the PDS confinement regime is obtained. Obviously, the gas concentrated at the centre would give rise to a secondary burst of star formation that would pump further energy into the super-SB.

Percolation of SBs in the adiabatic stage is likely to have a smaller effect, as the blast would continue to propagate into the hot phase. The cold phase would be affected by the relatively inefficient processes of thermo-evaporation and cloud dragging (preferentially in the radial direction). These same processes are in place also in presence of a hot phase that continually leaks out of the galaxy. In the adiabatic confinement regime the cold phase is so dense and with such a low filling factor that these effect are likely to

be inefficient, while in the case of adiabatic blow-out from a disc the dimensionality of the system would presumably lead to a funneling of the energy in the vertical direction, thus making a massive removal of gas unlikely.

As a matter of fact, the condition $Q_{\text{sb}} > 1$ is never met in the adiabatic confinement regime, while it is achieved in the critical cases discussed above (Fig. 8).

There are other cases in which the system may become critical. In presence of very high pressure the density of the cold phase can be so high (say $> 10^3 \text{ cm}^{-3}$) that the formation of H_2 is triggered even in absence of collapse. If this limit is reached when much gas is accumulated, this may give raise to a sudden burst of star formation.

Finally, a critical behaviour of the system can be triggered from outside. For instance, a strong tidal perturbation (or a merger) would act in two important ways, by lowering the Jeans mass of the clouds (because of the external pressure) and by thickening the structure, thus allowing a disc-like system to switch from adiabatic blow-out to adiabatic confinement; this would lower the Jeans mass even more and decrease the dynamical time. The effect would be a rapid consumption of the accumulated cold phase and a likely percolation of SBs.

5.3 Simplified models

The present model can be generalized to reproduce the components of real galaxies, like disc, bulge and halo, and then interfaced with a galaxy formation code that includes the mass assembly of dark-matter halos, cooling inside those halos, disc formation, galaxy mergers, interaction with galaxy clusters etc.. However, it is much more convenient to devise a set of approximate analytic solutions to this feedback model. These solutions can also be adapted to model the “sub-grid” physics of feedback in N-body simulations.

The solutions in the $H_{\text{eff}} - \Sigma_{\text{tot}}$ plane can be divided into four main regions where different regimes are met (adiabatic blow-out, adiabatic confinement, PDS confinement, critical blow-out cases). These regions are separated by limiting relations of the kind $\Sigma_{\text{tot}} = \Sigma_{\text{tot},0} (H_{\text{eff}}/1 \text{ kpc})^{-\alpha_{\text{lim}}}$, where the exponent α_{lim} is usually in the range 0.5–1. At the lowest densities (a factor 10^2 lower than Equation 55 for the reference choice of parameters) systems are critical, but they will most likely be kept ionized by the cosmological UV background, so they will simply not evolve. At densities below Equation 55 (again for the reference choice of parameters) the system is in the adiabatic blow-out regime. Above that limit it gets into the adiabatic confinement regime. PDS confinement is reached at densities higher than Equation 56 (valid for $E_{51}=0.3$ and $f_{\text{evap}}=0.05$).

For each regime a simplified solution can be obtained by noticing the following facts that are found to hold in most cases: 1) T_h is nearly constant, and equal to a value that mostly depends on the regime and on E_{51} ; 2) F_h , f_{coll} and f_c are nearly constant to values that mostly depend on the regime; 3) cooling is negligible in all cases but those in PDS confinement, where leak-out is negligible; 4) leak-out dominates over blow-out in non-critical cases if f_{bo} is not large. With these assumption it is relatively easy to solve the system of Equations 43 for the mass flows, while typical values of T_h , F_h , f_{coll} and f_c the different feedback regimes have been given in Section 4. However, a proper presenta-

tion of these simplified solutions requires some discussion that is out of place in this paper, so they will be presented elsewhere.

5.4 Limitations and further work

The merit of such relatively simple modeling is to highlight the possible physical regimes one should expect once a more complete calculation is performed. However, there are a number of limitations that have to be carefully taken into account to assess the validity of the results presented here.

(i) The Sedov solution for the SBs in the adiabatic stage is only a rough approximation of reality. There is a long list of effects, mentioned above and in part described by Ostriker and McKee (1988), that influence the dynamics of SBs. However, as long as the SBs expand in the relatively smoother hot component, it is likely that the Sedov solution gives the roughly correct evolution and functional dependences for the SBs.

(ii) As already mentioned, thermal conduction at the interface of cold and hot phases can make part of the cold gas evaporate. It has been verified that the impact of thermo-evaporation is small in the mass flows even if it is not quenched by magnetic fields, as the thermo-evaporated mass is usually smaller than the evaporated mass of the collapsing cloud whenever f_{evap} is not much smaller than one.

(iii) Type Ia SNe have not been considered. However, their introduction is straightforward in this model; they will interact directly with the ISM through a set of uncorrelated SNRs. As shown by Recchi et al. (2002), Type Ia SNe may be very important because they explode *after* a burst of star formation, and can contribute to maintain the hot phase when most cold gas is consumed.

(iv) Cosmic rays are known to be in rough equipartition with turbulence and magnetic fields. They are accelerated by the shocks generated by SNRs and SBs, directly or indirectly through turbulence (see, e.g., Longair, 1981). The role of cosmic rays, which are confined within the galaxy by magnetic fields, is that they distribute their energy to all the ISM, and not only to the densest collapsing clouds. So, they could give an important contribution to the mass and energy flows.

(v) There are other channels of mass and energy exchange between components that we are not considering here. One is the decay of turbulence driven by the kinetic energy of SNe, the other is the presence of a significant amount of mass in a warm phase, that can receive part of the energy of the blast and radiate it. Also, UV light coming from massive stars or from an external UV background could be responsible (together with thermo-evaporation) for continuous evaporation of the cold phase. Although some analytical estimates of these effects are possible, accurate numerical simulations will be necessary to assess the importance of these processes.

(vi) In realistic situations the ISM is subject to many influences, like spiral arms, differential rotation, tidal disturbances, mergers, ram pressure from hot halo gas (like in ellipticals or clusters) etc.. All these processes can be modeled once the global structure of the galaxy and its environment are specified. For instance, the passage of a spiral arm can be modeled by a periodic decrease of the Jeans mass due to the external pressure term. As in the adiabatic blow-out

case the coagulation time is $t_{\text{coag}} \sim 5 \times 10^7$ yr, of the same order of the frequency of spiral arms, the clouds have just time to coagulate to increase their mass by a factor of a few before the spiral arm sweeps again. So, a moderate decrease of the Jeans mass would suffice in guaranteeing that star formation takes place mainly in the spiral arms, even in absence of a more explicit connection, like that proposed by Ballesteros-Paredes et al. (1999).

(vii) The model presented here is assumed to be valid in the regime where many generations of collapsing clouds self-regulate in forming a galaxy. For dwarf galaxies some changes in the model are necessary: firstly it is important to check that at least one collapsing cloud is present; secondly, the first episode of star formation could itself cause a complete blow-away of the ISM (see, e.g., Ferrara & Tolstoy 2000), so that the system may never get into a self-regulated regime. Moreover, for dark matter halos with small circular velocities the leaked-out or blown-out gas will most likely be lost to the inter-galactic medium.

(viii) This model gives satisfactory predictions for the state of the ISM in a Milky Way-like situation. The high-density, bursting cases are subject to much weaker observational constraints, not only for the paucity of very nearby starbursts but also for the presence of dust that hampers observations in the optical, UV and soft-X bands. Besides, the extrapolation of the assumptions that are successful at low densities is not straightforward. For instance, large collapsing clouds could be generated in cooling flows or, as mentioned above, star formation could be triggered even in clouds smaller than the Jeans mass when thermal pressure makes them denser than a threshold density at which H₂ starts to form. Careful comparison with available observations is needed to constrain the parameters of feedback in the starburst cases.

(ix) This model can be improved to give more accurate predictions on observables related to the ISM. This would require proper (numerical) modeling of the intermediate warm phase(s) and of the ionization equilibrium between the phases.

5.5 Comparison with previous works

The model of the ISM of McKee & Ostriker (1977) has been a reference model for years, although the picture based on compressible supersonic MHD turbulence is now emerging. The model presented here has many points in common with McKee & Ostriker (1977), but presents many improvements: (i) we address the dynamics of the ISM, including star formation and feedback; (ii) we assume no equilibrium, but investigate on the conditions that lead to self-regulated or critical ISM; (iii) we take into account the correlated nature of Type II SNe. Besides, we do not consider the warm phase and its ionization equilibrium with the hot phase. In the present model we do not require unit porosity of SBs to justify its presence of a hot phase (which sometimes cannot even be maintained). As a matter of fact, unit porosity of SBs is hardly reached in non-critical cases; however, uncorrelated adiabatic SNRs that stop at R_{bo} would have a porosity of order one in the MW example, but not in the EL one in the adiabatic confinement case. So, on the light of the present results, $Q = 1$ is at best an unnecessary assumption.

Some recent works on galaxy formation by Silk (1997;

2000), Efthathiou (2000), Shu, Mo & Mao (2003) or Springer & Hernquist (2003) present models of feedback and star formation based at least in part on the McKee & Ostriker (1977) model. In these cases Type II SNe are assumed to be uncorrelated and the ISM is assumed to be self-regulated to a unit value of the porosity of SNRs. For instance, Efthathiou (2000) fixes the star formation by assuming equilibrium between the kinetic energy acquired by cold clouds at shocks and that lost by coagulation, while Silk (1997, 2000) connects star formation to the dynamics of the disc by requiring the Toomre Q -parameter to be unity and postulating the identity of the time scale for star formation with the viscous time scale; this is an important ingredient for obtaining exponential discs, but the nature of this identity remains unexplained. The model presented here does not assume any equilibrium, and does not use any ingredient of disc dynamics, thus being applicable in virtually all situations. While it is clear that disc dynamics will influence the evolution of a spiral galaxy, our results suggest that most properties of galaxy formation can be understood simply as a chain of local processes.

An alternative to the present modeling is to consider the ISM as turbulent. As shown by Avila-Reese & Vazquez-Semadeni (2001) the ISM can be considered as a globally turbulent medium, with turbulence forced in specific places (the star-forming regions) and propagating throughout the volume. The “diffusion” velocity of turbulence is connected to the time scale of decay of turbulence. Both this group, that uses a 2D code, and Mac Low et al. (1998), who use a 3D code, find that turbulence decays as $t^{-\alpha}$ with $\alpha \simeq 0.8$. It is easy to show that (Avila-Reese & Vazquez-Semadeni 2001), when turbulence is forced in some specific sites, the rms velocity of turbulence scales with distance from the forcing region as $u_{\text{rms}} \propto l^{-\alpha/(2-\alpha)}$, while the decay distance of turbulence grows with time as $l \propto t^{1-\alpha/2}$. It is remarkable that for $\alpha = 0.8$ the two exponents are exactly equal to our relations $R_{\text{sb}} \propto t^{0.6}$ and $v_{\text{sb}} \propto R^{-0.4}$. While a direct physical interpretation of this fact may be misleading without further investigation, it is clear that the propagation of energy through the ISM by isolated spherical blasts is not in clear contradiction with the results of the turbulent model. This confirms the validity of a simple treatment as a first approximation.

6 CONCLUSIONS

We have presented a model for feedback in galaxy formation, based on a two-phase ISM, that does not restrict to self-regulated, equilibrium solutions and neglects (for simplicity) the global structure of the galaxy, apart from its density, vertical scale-height and velocity dispersion of clouds. From the dynamics of the SBs that arise from the collapsing “molecular” clouds, we have identified four possible regimes of feedback, depending on whether SBs blow out of the “disc” or remain pressure-confined, and whether they have time to enter the PDS stage. For a reference set of parameter values we have studied the dynamics of the system in the vertical scale-height – surface density plane, identifying the regions of the plane corresponding to different regimes. Both blow-out and confinement mostly take place in the adiabatic regime. In a Milky Way-like adiabatic blow-out case, the main charac-

teristics of the ISM of the Galaxy are broadly reproduced. In the adiabatic confinement regime the ISM is predicted to have higher pressure, temperature of hot phase and densities of both phases, and smaller collapsing clouds; in some cases the density of the cold phase could be high enough to trigger diffuse star formation. PDS confinement is found for high-density, thick structures in significant regions of the parameter space. In this case feedback is less effective, the hot phase cooler and star formation quicker.

In many cases the system becomes critical, in the sense that the hot phase is severely depleted and the cold phase percolates the whole volume. This happens for very low-density thin systems (that would however be kept ionized by the cosmological UV background), in some regions of the parameter space also for low-density thick systems in adiabatic blow-out (that may correspond to some gas-rich dwarf galaxies) and for high-density thick systems in PDS confinement (that may correspond to high-redshift galaxies). The most likely result of this critical behaviour is the sudden consumption by star formation of the cold gas accumulated by the galaxy; the dynamics switches from a “candle”- to a “bomb”-like solution.

The porosity of SBs is usually found to be much lower than unity. However, in some cases unit porosity is found while SBs are in the PDS stage. This corresponds to the formation of a super-SB that sweeps the whole galaxy, removing most ISM from it. These events, together with the critical solutions, are likely connected to the triggering of galactic winds.

With respect to previous models of feedback, the main parameters that are typically present, as the efficiency of feedback, the Schmidt law with its normalization, or the rate of blow-out and leak-out of gas from a star-forming galaxy, are predictions of the present model. The parameter space is connected to the properties of the ISM, and can thus be constrained by observations of the Milky Way and nearby galaxies; most parameters can be fixed in principle by reproducing only the Milky Way. Moreover, the mass flows used in this model can be fine tuned by comparing with future detailed simulations of the ISM in a forming galaxy that include all the main physical processes though to be at work.

This model does not restrict to self-regulated ISM, and presents a rich variety of solutions with a relatively limited set of parameters. Although the turbulent nature of the ISM is not explicitly taken into account, the model is thought to give a good approximation to the solution of the feedback problem. The feedback regimes found here can be used, together with the refinements of the model that will be given in upcoming papers, to construct a realistic grid of feedback solutions to be used in galaxy formation codes, either semi-analytic or numeric.

ACKNOWLEDGMENTS

The author thanks Andrea Ferrara, Gianrossano Giannini, Gabriele Cescutti and especially Simone Recchi for many fruitful discussions.

REFERENCES

Avila-Reese, V., Vazquez-Semadeni, E., 2001, *ApJ*, 553, 645
 Ballesteros-Paredes, J., Vazquez-Semadeni, E., Scalo, J., 1999, *ApJ* 515, 286
 Bonnor, W.B., 1956, *MNRAS*, 116, 351
 Castor, J., McCray, R., Weaver, R., 1975, *ApJ*, 200, L107
 Cavaliere, A., Colafrancesco, S., Menci, N., 1991, *ApJ*, 376, L40
 Cavaliere, A., Colafrancesco, S., Menci, N., 1992, *ApJ*, 392, 41
 Chappell, D., Scalo, J., 2001, *ApJ*, 551, 712
 Chiappini, C., Matteucci, F., Romano, D., 2001, *ApJ*, 554, 1044
 Chiosi, C., Carraro, G., 2002, *MNRAS*, 335, 335
 Cioffi, D.F., McKee, C.F., Bertschinger, E., 1988, *ApJ*, 334, 252
 Cole, S., Lacey, C.G., Baugh, C.M., Frenk, C.S., 2000, *MNRAS*, 319, 168
 de Young, D.S., Gallagher, J.S.III, 1990, *ApJ*, 356, L15
 Diaferio, A., Kauffmann, G., Balogh, M.L., White, S.D.M., Schade, D., Ellingson, E., 2001, *MNRAS*, 323, 999
 Ebert, R., 1955, *Z. ApJ*, 37, 217
 Efstathiou, G., 2000, *MNRAS*, 317, 697
 Elmegreen, B.G., 2000, *ApJ*, 530, 277
 Elmegreen, B.G., 2002, *ApJ*, 564, 773
 Ferguson, H.C., van Dike Dixon, W., Davidsen, A.F., Dettmar, R.-J., 1995, *ApJ*, 454, L23
 Ferrara, A., Tolstoy, E., 2000, *MNRAS*, 313, 291
 Ferreras, I., Scappapietra, E., Silk, J., 2002, *ApJ*, 579, 247
 Franco, J., Shore, S.N., Tenorio-Tagle, G., 1994, *ApJ*, 436, 795
 Fraternali, F., Cappi, M., Sancisi, R., Oosterloo, T., 2002, *ApJ*, 578, 109
 Governato, F., Mayer, L., Wadsley, J., Gardner, J.P., Willman, B., Hayashi, E., Quinn, T., Stadel, J., Lake, G., 2004, *ApJ*, in press (astro-ph/0207044)
 Hatton, S., Devriendt, J.E.G., Ninin, S., Bouchet, F.R., Guiderdoni, B., Vibert, D., 2003, *MNRAS* 343, 75
 Heiles, C., 2001, in “Galactic Structure, Stars and the Interstellar Medium”, eds. C.E. Woodward, M.D. Bicay, & J.M. Shull, ASP Conference Series, Vol. 231 (ASP: San Francisco). p.294
 Hirashita, H., Burkert, A., Takeuchi, T.T., 2001, *ApJ*, 552, 591
 Jenkins, E.B., 2002, in Chemical Enrichment of Intracluster and Intergalactic medium, eds. R. Fusco-Femiano & F. Matteucci, ASP Conf. Ser., vol. 253. Pag 365
 Kennicutt, R.C., 1989, *ApJ*, 344, 685
 Koo, B.-C., McKee, C.F., 1992, *ApJ*, 388, 93
 Kritsuk, A., Norman, M.L., 2002, *ApJ*, 569, L127
 Lia, C., Portinari, L., Carraro, G., 2002, *MNRAS*, 330, 821
 Lin, D.N.C., Murray, S.D., 2000, *ApJ*, 540, 170
 Lombardi, M., Bertin, G., 2001, *A&A*, 375, 1091
 Longair, M., 1981, High Energy Astrophysics, Cambridge University Press
 Mac Low, M.-M., Klessen, R.S., Burkert, A., Smith, M.D., 1998, *PRL*, 80, 2754
 Mac Low, M.-M., McCray, R., 1988, *ApJ*, 324, 776
 Mac Low, M.-M., McCray, R., Norman, M.L., 1989, *ApJ*, 337, 141

Mac Low, M.-M., 2003, in “Simulations of magnetohydrodynamic turbulence in astrophysics”, eds. E. Falgarone & T. Passot, Springer. pag. 182

Mathis, H., Lemson, G., Springel, V., Kauffmann, G., White, S.D.M., Eldar, A., Dekel, A., 2002, MNRAS, 333, 739

Matzner, C.D., 2002, ApJ, 566, 30

McKee, C.F., Ostriker, J.P., 1977, ApJ, 218, 148

McKee, C.F., van Buren, D., Lazareff, B., 1984, ApJ, 278, L115

Menci, N., Cavalieri, A., Fontana, A., Giallongo, E., Poli, F., 2002, ApJ, 575, 18

Monaco, P., 2002, in Chemical Enrichment of Intracluster and Intergalactic medium, eds. R. Fusco-Femiano & F. Matteucci, ASP Conf.Ser., vol. 253. Pag 279

Monaco, P., 2003, in Galaxy Evolution: Theory and Observations, eds. V. Avila-Reese, C. Firmani, C. Frenk, & C. Allen, RevMexAA 17, 71

Monaco, P., 2004, submitted to MNRAS (paper II)

Mori, M., Ferrara, A., Madau, P., 2002, ApJ 571, 40

Ostriker, E.C., Gammie, C.F., Stone J.M., 1999, ApJ, 513, 259

Ostriker, J., McKee, C.F., 1988, Rev.Mod.Phys., 60, 1

Pearce, F. R., Jenkins, A., Frenk, C.S., White, S.D.M., Thomas, P.A., Couchman, H.M.P., Peacock, J.A., Efstathiou, G., 2001, MNRAS, 326, 649

Poli, F., Menci, N., Giallongo, E., Fontana, A., Cristiani, S., D’Odorico, S., 2001, ApJ, 551, L45

Press, W.H., Teukolsky, S.A., Vetterling, W.T., Flannery, B.P., 1992, Numerical recipes in FORTRAN, Cambridge: University Press

Recchi, S., Matteucci, F., D’Ercole, A., Tosi, M., 2002, A&A, 384, 799

Saslaw, W.C., 1985, Gravitational Physics of Stellar and Galactic Systems (Cambridge: Cambridge University Press)

Savage, B.D., Sembach, K.R., Jenkins, E.B., et al., 2000, ApJ, 538, L27

Schaye, J., 2004, ApJ, in press (astro-ph/0205125)

Schmidt, M., 1959, ApJ, 129, 243

Shu, C., Mo, H.J., Mao, S., 2002, submitted to MNRAS (astro-ph/0301035)

Silk, J., 1997, ApJ, 481, 703

Silk, J., 2001, MNRAS, 324, 313

Solomon, P.M., Rivolo, A.R., Barrett, J., Yahil, A., 1987, ApJ, 319, 730

Somerville, R.S., Primack, J.R., Faber, S.M., 2001, MNRAS, 320, 504

Springel, V., Hernquist, 2003, MNRAS 339, 289

Steinmetz, M., Navarro, J.F., 2002, NewA, 7, 155

Strickland, D.K., Heckman, T.M., Weaver, K.A., Hoopes, C.G., Dahlem, M., 2002, ApJ, 568, 689

Tan, J.C., 2000, ApJ, 536, 173

Toft, S., Rasmussen, J., Sommer-Larsen, J., Pedersen, K., 2002, MNRAS, 335, 799

Tornatore, L., Borgani, S., Springel, V., Matteucci, F., Menci, N., Murante, G., 2003, MNRAS 342, 1025

Vazquez-Semadeni, E., 2002, in “Seeing Through the Dust: The Detection of HI and the Exploration of the ISM in Galaxies”, eds. R. Taylor, T. Landecker, & A. Willis; ASP: San Francisco. Pag. 155 (A larger version available in astro-ph/0201072)

von Smoluchowski, M., 1916, Phys. Z., 17, 557

Weaver, R., McCray, R., Castor, J., Shapiro, P., Moore, R., 1977, ApJ, 218, 377

Weinberg D.H., Hernquist L., Katz N., 2002, ApJ, 571, 15

Williams, J.P., McKee, C.F., 1997, ApJ, 476, 166

APPENDIX A: LIST OF FREQUENTLY USED SYMBOLS

α_{cl}	Slope of mass function of clouds
a_{cl}	Radius of cloud
$c_{\text{s,h}}$	Sound speed of the hot phase
E_{51}	Energy released by a SN
$E_{\text{sb}}^{(\text{th})}$	Thermal energy of a SB
$E_{\text{sb}}^{(\text{kin})}$	Kinetic energy of a SB
\dot{E}_{sn}	Rate of energy release from SNe
\dot{E}_{cool}	Rate of energy loss by cooling
\dot{E}_{snpl}	Rate of energy loss by snowplows
\dot{E}_{bo}	Rate of energy loss by blow-out
\dot{E}_{leak}	Rate of energy loss by leak-out
\dot{E}_{fb}	Rate of energy gain from SBs
\dot{E}_{hot}	Net energy flux of the hot phase
f_{E}	Efficiency of feedback
$f_{\text{h}}, f_{\text{c}}$	Filling factors of the two phases
f_{coll}	Fraction of cold gas in collapsing clouds
f_{\star}	Efficiency of star formation
f_{evap}	Evaporated fraction of collapsed cloud
f_{bo}	Fraction of swept gas blown out by a SB
$f_{\text{bo,max}}$	Largest value of f_{bo}
f_{cool}	Fraction of cooled gas in a cooling flow
f_{rest}	Fraction of restored mass
f_{pds}	Release of energy after PDS confinement
F_{h}	Fraction of hot gas
H_{eff}	Vertical scale-height of the system
$H_{\text{eff,h}}$	Dynamical vertical scale-height of hot gas
H_{h}	Height of the layer of hot leaked-out gas
L_{38}	Mechanical luminosity of a SB
m_{cl}	Mass of clouds
m_{l}	Lower cutoff mass of clouds
m_{u}	Upper cutoff mass of clouds
m_{J}	Jeans mass of clouds
m_{cc}	Mass of the collapsing cloud
M_{sw}	Mass swept by a SB
M_{int}	Swept mass that is still hot inside a SB
$M_{\star,\text{sn}}$	Mass of formed stars per SN
M_{tot}	Total mass of the system
M_{i}	Mass of the i component*
M_{i}^Z	Mass of metals in the i component*
\dot{M}_{i}	Net mass flux of the i component*
\dot{M}_{i}^Z	Net metal flux of the i component*

\dot{M}_{inf}	Infall rate
\dot{M}_{cool}	Cooling rate
\dot{M}_{leak}	Leak-out rate
\dot{M}_{sf}	Star formation rate
\dot{M}_{rest}	Restoration rate
\dot{M}_{evap}	Evaporation rate
\dot{M}_{int}	Sweeping rate minus snowplow rate
\dot{M}_{snpl}	Snowplow rate
μ_h, μ_c	Molecular weights of the two phases
μ_{shape}	Shape parameter for collapsing clouds
n_h, n_c	Density of the two phases
N_{cl}	Mass function of clouds
N_{cc}	Total number of collapsing clouds
N_{sn}	Number of SNe in a collapsing cloud
P	Pressure of the ISM
Q_{sb}	Porosity of SBs
R_{sb}	Radius of SB
R_{pds}	Radius of shell collapse for a SB
R_{conf}	Confinement radius of a SB
$R_{\text{bo'}}$	Final radius of a blown-out unconfined SB
R_{fin}	Final radius of a SB
R_{sn}	Rate of SN explosions in a collapsing cloud
ρ_{tot}	Total density of the system
$\bar{\rho}_h, \bar{\rho}_c$	Average densities of the two phases
σ_v	Velocity dispersion of clouds
Σ_{tot}	Total surface density of the system
t_{coag}	Coagulation time
t_{dyn}	Dynamical time of clouds
t_{cool}	Cooling time of hot gas
t_{cross}	Sound crossing-time of a SB
t_{pds}	Time of shell collapse for a SB
t_{conf}	Confinement time for a SB
t_{life}	Lifetime of an $8 M_{\odot}$ star
t_{bo}	Time of first blow-out of a SB
$t_{\text{bo'}}$	Final time of a blown-out unconfined SB
t_{fin}	Final time of a SB
t_{inf}	Infall time scale
t_{leak}	Leak-out time scale
t_{sf}	Star-formation time scale
T_h, T_c	Temperature of the two phases
T_{evap}	Temperature of evaporated mass
v_{sb}	Velocity of SB
y	Yield from massive stars
Z_i	Metallicity of the i component*
ζ_m	Metallicity in solar units
Notes:	
* $i = \text{hot, cold, } \star, \text{ halo}$	

APPENDIX B: TIME-SCALES FOR THE COAGULATION OF COLD CLOUDS

We obtain here the time-scales for coagulation, given in Section 2.4, from the Smoluchowski equation of kinetic aggregations. This demonstration follows Cavaliere et al. (1992). The Smoluchowski evolution equation for the mass function of clouds $n(m; t)$ is:

$$\frac{\partial n}{\partial t} = \frac{1}{2} \int_0^m dm' K(m', m - m') n(m'; t) n(m - m'; t)$$

$$-n(m; t) \int_0^\infty dm' K(m, m') n(m'; t). \quad (\text{B1})$$

The kernel for aggregations of clouds 1 and 2, $K(m_1, m_2)$ is given by Equation 9, where the cross-section for interactions is given by Equation 10. We define a typical mass for the mass function m_* (which is then identified with the upper cutoff m_u) and scale all masses with m_* through the unidimensional variable $\nu = m/m_*$. We separate the kernel for aggregation of clouds into geometric and resonant terms (the latter term being considered only in this appendix), and write the two terms as follows:

$$\begin{aligned} K_{\text{geom}} &= \mathcal{F}_{\text{geom}} m_*^{2/3} \langle (\nu_1^{1/3} + \nu_2^{1/3})^2 \rangle_m \\ K_{\text{res}} &= \mathcal{F}_{\text{res}} m_*^{4/3} \langle (\nu_1 + \nu_2) (\nu_1^{1/3} + \nu_2^{1/3}) \rangle_m. \end{aligned} \quad (\text{B2})$$

We call λ the exponent of m_* in the equations. The two \mathcal{F} functions are respectively $\mathcal{F}_{\text{geom}} = \bar{\rho}_c \pi (4\pi \rho_c/3)^{-2/3} \langle v_{\text{ap}} \rangle_v$ and $\mathcal{F}_{\text{res}} = \bar{\rho}_c 2\pi G (4\pi \rho_c/3)^{-1/3} \langle (v_{\text{ap}})^{-1} \rangle_v$. Let's assume that the mass function is expressible as:

$$n(m; t) dm = m_*^2 \Phi(\nu) d\nu. \quad (\text{B3})$$

This is valid if the slope of the mass function is fixed and if $m_1 \ll m_u$. Inserting this *ansatz* into the Smoluchowski equation, and considering only the time-dependent terms, we easily obtain the equation:

$$\dot{m}_* = \mathcal{F} m_*^\lambda. \quad (\text{B4})$$

This is valid for the two coagulation modes. This equation admits the solution:

$$m_*(t) = m_{*0} (1 - (\lambda - 1) \mathcal{F} m_{*0}^{\lambda-1} (t - t_0))^{1/(1-\lambda)}. \quad (\text{B5})$$

We can then define a coagulation time as $t_{\text{coag}} = 1/\mathcal{F} m_{*0}^{\lambda-1}$. For the two coagulation modes we obtain:

$$\begin{aligned} m_*(t) &= m_{*0} \left(1 + \frac{t - t_0}{3t_{\text{coag}}} \right)^3 \quad (\text{GEOM.}) \\ m_*(t) &= m_{*0} \left(1 - \frac{t - t_0}{3t_{\text{coag}}} \right)^{-3} \quad (\text{RES.}). \end{aligned} \quad (\text{B6})$$

It is easy to verify that the coagulation time is given by Equation 11 in the case of geometrical interactions, while in the resonant case:

$$t_{\text{coag}} = \left(\frac{4\pi}{3} \right)^{1/3} \frac{1}{2\pi G} \bar{\rho}_c^{-2/3} \frac{\rho_c}{\bar{\rho}_c} \frac{1}{m_j^{1/3} \langle (v_{\text{ap}})^{-1} \rangle}. \quad (\text{B7})$$

Finally, it is worth noticing that the slope of the mass function is assumed not to change during the evolution of the system, while coagulation would in general imply a flattening of the mass function. This is reasonable in cases where coagulation and collapse regulate the mass function to a given shape.

APPENDIX C: FEEDBACK REGIMES IN THE n_h – L_{38} PLANE

The fate of the SB depends mostly on the hot phase density n_h and the mechanical luminosity L_{38} . To better quantify the fate of the SB we restrict to the case of solar metallicity and $\mu_h = 0.6$, and express the hot phase density in units

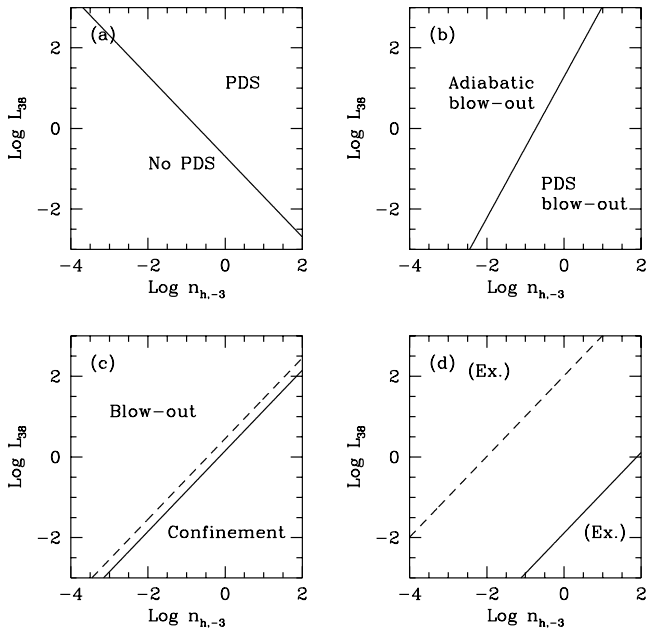


Figure C1. Fate of SBs in the n_h – L_{38} plane. The panels indicate the lines separating the domains in which SBs (a) get or do not get into the PDS stage, (b) blow-out in the adiabatic or PDS stage, (c) blow out or remain confined, (d) end after exhaustion of SNe.

of $n_{h,-3} = n_h/(10^{-3} \text{ cm}^{-3})$. Moreover, H_{eff} is expressed in units of 10^3 pc and the temperature of the hot phase in units of 10^6 K . Table C1 reports the characteristic times of SBs.

It is useful to analyse the fate of SBs in the n_h – L_{38} plane. The condition $t_{\text{pds}} = t_{\text{conf}}^{(\text{ad})}$ determines the possibility of getting into the PDS stage; it is equivalent to the line:

$$L_{38} = 0.20 T_{h,6}^{11/2} n_{h,-3}^{-1}. \quad (\text{C1})$$

In absence of blow-out, below this line SBs are pressure-confined in the adiabatic stage, above this line they can go into the PDS stage (Fig. C1a). The condition $t_{\text{pds}} = t_{\text{bo}}$ determines whether the blow-out is in the adiabatic or PDS stage; it is equivalent to:

$$L_{38} = 19 H_{\text{eff},3}^{11/4} n_{h,-3}^{7/4}. \quad (\text{C2})$$

In case of blow-out, to the left of this line SBs blow out in the adiabatic stage (which is maintained even after one sound crossing time), to the right of it SBs blow out in the PDS stage (Fig. C1b). The condition $t_{\text{bo}} = t_{\text{conf}}$ determines whether SBs are going to end by blow-out or confinement; in the adiabatic stage it is equivalent to:

$$L_{38} = 1.4 H_{\text{eff},3}^2 T_{h,6}^{3/2} n_{h,-3}. \quad (\text{C3})$$

In the PDS stage the numerical factor is 2.9. Below this line SBs are pressure-confined, above it they blow out (Fig. C1c).

Fig. C2 shows all the relations listed above and the regions they define in the n_h – L_{38} plane for the choice $T_h = 10^6 \text{ K}$ and $H_{\text{eff}} = 10^3 \text{ pc}$. The thick lines mark the boundaries of regions where SBs end in a different way. Region (1) in the figure contains the SBs that blow out in the adiabatic stage. In region (2) SBs are confined in the adiabatic stage, while in region (3) SBs are confined in the PDS stage. In

t_{pds}	$= 2.87 \times 10^6 L_{38}^{3/11} n_{h,-3}^{-8/11} \mu_{h,0.6}^{9/22} \zeta_m^{-5/11} \text{ yr}$	
R_{pds}	$= 674 L_{38}^{4/11} n_{h,-3}^{-7/11} \mu_{h,0.6}^{1/22} \zeta_m^{-3/11} \text{ pc}$	
t_{conf}	$= 4.12 \times 10^6 L_{38}^{1/2} n_{h,-3}^{-1/2} \mu_{h,0.6}^{3/4} T_{h,6}^{-5/4} \text{ yr}$	(ad.)
	$= 2.95 \times 10^6 L_{38}^{1/2} n_{h,-3}^{-1/2} \mu_{h,0.6}^{3/4} T_{h,6}^{-5/4} \text{ yr}$	(PDS)
R_{conf}	$= 857 L_{38}^{1/2} n_{h,-3}^{-1/2} \mu_{h,0.6}^{1/4} T_{h,6}^{-3/4} \text{ pc}$	(ad.)
	$= 592 L_{38}^{1/2} n_{h,-3}^{-1/2} \mu_{h,0.6}^{1/4} T_{h,6}^{-3/4} \text{ pc}$	(PDS)
t_{bo}	$= 5.53 \times 10^6 L_{38}^{-1/3} n_{h,-3}^{1/3} \mu_{h,0.6}^{1/3} H_{\text{eff},3}^{5/3} \text{ yr}$	(ad.)
	$= 7.06 \times 10^6 L_{38}^{-1/3} n_{h,-3}^{1/3} \mu_{h,0.6}^{1/3} H_{\text{eff},3}^{5/3} \text{ yr}$	(PDS)
R_{bo}	$= 10^3 H_{\text{eff},3} \text{ pc}$	
$t_{\text{bo}'}$	$= 3.11 t_{\text{bo}}$	(ad)
	$= 2.81 t_{\text{bo}}$	(PDS)
$R_{\text{bo}'}$	$= 1.98 R_{\text{bo}}$	(ad)
	$= 1.86 R_{\text{bo}}$	(PDS)

Table C1. Characteristic times of a SB for typical values of the parameters. Here $\mu_{h,0.6} = \mu_h/0.6$.

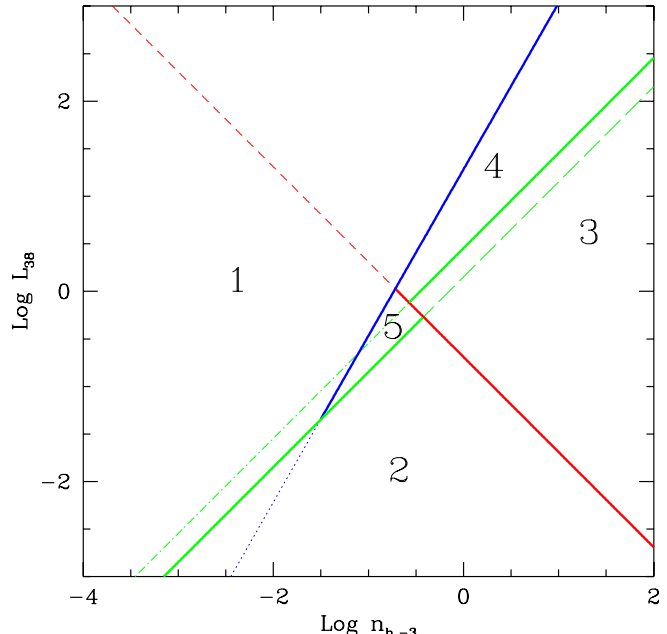


Figure C2. As in Fig. C1, but with all lines drawn together. For the explanations of the five regions, see the text.

region (4) SBs blow out in the PDS stage. Finally, in the closed region (5) SBs blow out in the adiabatic stage, but are confined before one sound crossing time. For other values of H_{eff} and T_h the lines move along the plane, but it is easy to check that the area of the triangle corresponding to region (5) is invariant.

It is interesting also to consider the region of the parameter space in which SBs end after all SNe have exploded. This happens when $t_{\text{bo}} = t_{\text{life}}$ and $t_{\text{conf}} = t_{\text{life}}$. The two conditions give:

$$\begin{aligned} L_{38} &= 6.2 \times 10^{-3} H_{\text{eff},3}^5 n_{h,-3} \\ L_{38} &= 1.9 \times 10^2 T_{h,6}^{5/2} n_{h,-3}. \end{aligned} \quad (\text{C4})$$

They are both satisfied below the first line and above the second (Fig. C1d). As the two lines are parallel, this happens only if $H_{\text{eff},3}T_{h,6}^{-1/2} = 7.9$. In this case a whole band in the plane corresponds to exhaustion.

We conclude this discussion by noting that the plane is not uniformly populated, as both n_h and L_{38} are dynamical variables. In other words, the probability of a certain regime is not determined by the area occupied in the plane but by the dynamics of the system.

This paper has been typeset from a \TeX / \LaTeX file prepared by the author.